Digestive Diseases and Sciences (2018) 63:1102–1122
https://doi.org/10.1007/s10620-018-4991-x

PARADIGM SHIFTS IN PERSPECTIVE

Contributions of Magnetic Resonance Imaging to Gastroenterological Practice: MRIs for GIs

Christopher G. Roth[1] · Dina Halegoua-De Marzio[1] · Flavius F. Guglielmo[1]

Published online: 16 March 2018

Abstract
MRI has transformed from the theoretical, investigative realm to mainstream clinical medicine over the past four decades and has become a core component of the diagnostic toolbox in the practice of gastroenterology (GI). Its success is attributable to exquisite contrast and the ability to isolate specific proton species through the use of different pulse sequences (i.e., T1-weighted, T2-weighted, diffusion-weighted) and exploiting extracellular and hepatobiliary contrast agents. Consequently, MRI has gained preeminence in various GI clinical applications: liver and pancreatic lesion evaluation and detection, liver transplantation evaluation, pancreatitis evaluation, Crohn's disease evaluation (using MR enterography) rectal cancer staging and perianal fistula evaluation. MR elastography, in concert with technical innovations allowing for fat and iron quantification, provides a noninvasive approach, or "MRI virtual liver biopsy" for diagnosis and management of chronic liver diseases. In the future, the arrival of ultra-high-field MR systems (7 T) and the ability to perform magnetic resonance spectroscopy in the abdomen promise even greater diagnostic insight into chronic liver disease.

Keywords Magnetic resonance imaging · Elastography · Enterography · T1-weighted · T2-weighted · Diffusion-weighted · Gadolinium · Radiofrequency · Liver · Pancreas · LI-RADS

Introduction

In less than four decades since its invention, magnetic resonance imaging (MRI) has been transformed from a tool mostly limited to investigative applications to a core component of the diagnostic armamentarium in modern medicine. In the USA, over 100 MRI examinations have been performed per 1000 people since 2010 [1]. While early MRI technology focused on the brain, the spine, and the joints, primarily since physiologic movement thwarted imaging of other organs, today's MR systems are capable of acquiring high-quality images of the abdomen and pelvis for numerous applications, especially pertaining to the gastrointestinal (GI) system. Moreover, MRI has become integral to the practice of gastroenterology in numerous instances such as characterizing liver lesions, managing patients with chronic liver disease and potential liver transplant recipients, quantifying chronic liver disease, diagnosing and assessing biliary diseases, establishing the etiology and potential complications of pancreatitis, diagnosing pancreatic cancer, managing Crohn's disease and polyposis syndromes, detecting perianal fistulas, and staging rectal cancer. Future directions depend on the potential applications of ultra-high-field MRI (i.e., 7 T) initially in the direction of better understanding hepatic energy metabolism through enhanced spectroscopic capabilities at higher field strength—specifically by analyzing phosphorus metabolites.

This article reviews the history, current state, and future direction for MR scanning as pertains to gastroenterologists. Part of its purpose is to describe how paradigm shifts in particle physics transformed medical practice decades later; the other is to provide insight into a field that is not always well understood by GI specialists. The authors hope that this insight into the enormous capabilities of MR for imaging the GI tract will not only enhance appreciation of the study in its many forms, but also reinforce the importance of practitioners providing as much clinical information as possible when ordering such studies.

✉ Christopher G. Roth
Christopher.Roth@jefferson.edu

[1] Department of Radiology, Thomas Jefferson University, Philadelphia, USA

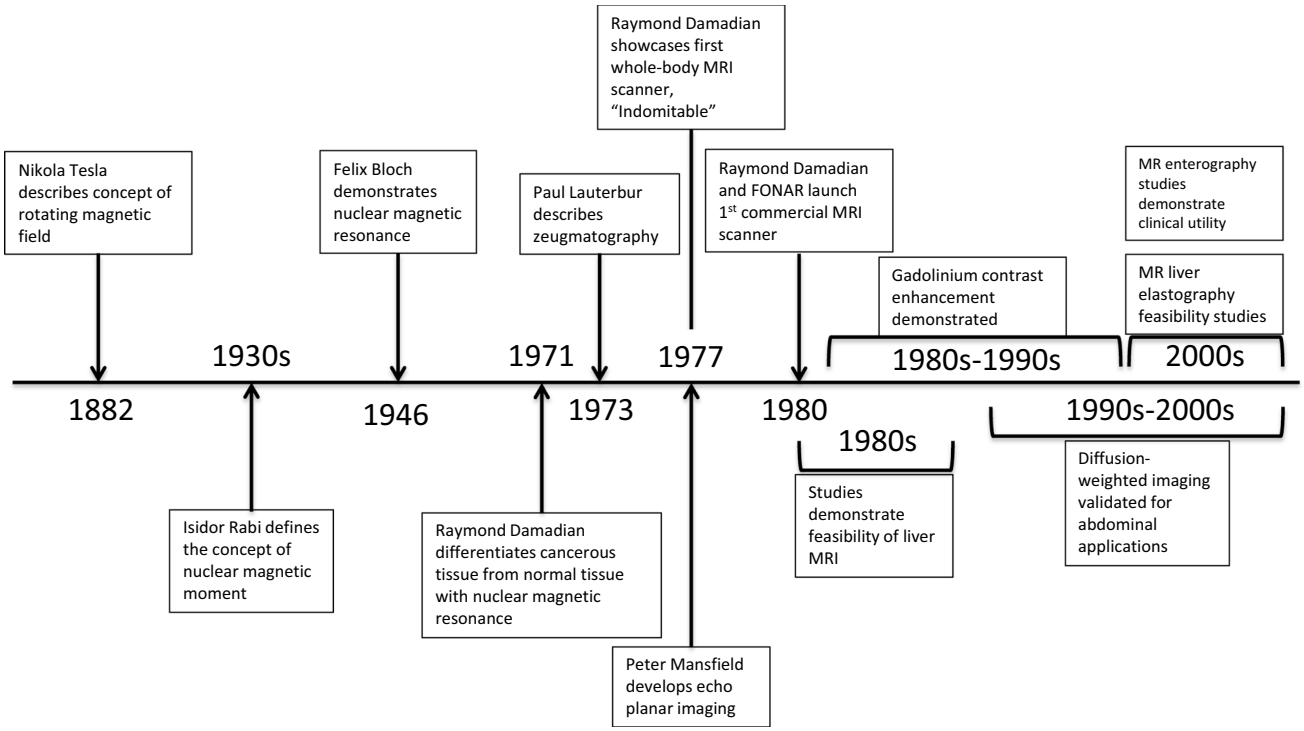

Fig. 1 Timeline of important developments in MRI and gastrointestinal applications

History of MRI

The earliest known discovery to which the development of clinical MRI can be credited is Nikola Tesla's concept of the rotating magnetic field, first described in 1882 in Budapest, Hungary (Fig. 1). This phenomenon involves exploiting the ability of multiple magnetic fields to separate protons based on their chemical species and spatial location. Nevertheless, multiple convergent subsequent scientific discoveries were needed in order to usher in the advent of clinical magnetic resonance imaging. The world would have to wait over a half century for the next major innovation—nuclear magnetic resonance (NMR), the basis of current MRI imaging. The independent contributions from Columbia University Professor Isidor I. Rabi and the team of Edward Purcell and Felix Bloch provided the scientific understanding of this phenomenon through their respective discoveries. In the 1930s, Rabi elucidated the concept of the magnetic moment, the notion that protons or other atomic nuclei have the capacity to behave as tiny magnets, absorbing and emitting energy when subjected to radiofrequency energy. In 1946, Felix Bloch and his team demonstrated the phenomenon of NMR in matter by measuring the radiofrequency energy in voltage emitted by water subjected to a rotating magnetic field.

Three more decades would elapse before a combination of scientific discoveries, and technological innovations would converge to transform the understanding of this physical phenomenon into its practical application—magnetic resonance imaging (MRI) as is currently termed. Raymond Dalmatian, a physician and mathematician at Downstate Medical Center, used NMR to demonstrate a difference in emitted radiofrequency energy between the protons in explanted normal and malignant tissues in rats in 1971 [2]. Paul Lauterbur, a chemistry professor at SUNY Stonybrook, appreciated the value of Damadian's work and the need to translate this technological innovation to an *in vivo* environment. In his seminal work entitled, "Image Formation by Induced Local Interactions: Examples Employing Nuclear Magnetic Resonance," he described how the addition of a second magnetic field enabled spatial localization and image creation (i.e., "zeugmatography"), obviating the need to remove tissue from the body in order to potentially obtain diagnostic images [3]. Peter Mansfield, a British physicist, concurrently worked on how to mathematically analyze the signals generated with interacting gradient magnetic fields, developing a novel system for rapidly obtaining magnetic resonance images, known as echo planar imaging [4]. Meanwhile, Damadian was awarded a patent for his "Apparatus for Detecting Cancer in Tissue" in 1974, which led to his development of the first whole-body MRI scanner in 1977 named "Indomitable." In 1980, Damadian formed the Fonar Corporation, introducing the first commercial

MRI scanner. Ultimately, Lauterbur and Mansfield won the Nobel Prize in Physiology or Medicine in 2003 for their synergistic discoveries, although Damadian's discoveries and innovations were arguably equally important and were definitely financially rewarding, with the Damadian-owned Fonar Corporation currently valued at over $180 million.

Since the 1970s, MRI has evolved technologically in a number of ways. New pulse sequences (the scripted way in which the magnetic field gradients are turned on and off) have been devised that enable faster imaging and more efficient means to collect MRI signals. Magnetic field gradient performance (the speed at which they ramp up and down) has escalated substantially, enabling faster imaging and newer applications able to accommodate physiologic motion such as cardiac pulsation, respiratory motion, and bowel peristalsis. Coil technology (the radiofrequency energy signal transmitter and receiver) has continuously evolved in order to enhance the quantity and richness of the MRI signal, with consequent enhanced quality of MR images. Hardware improvements have enabled higher-field imaging (1.5 T and above), which improves image quality and facilitates more challenging MR applications such as cardiac, abdominal, vascular, and diffusion-weighted imaging, and wider, more open configuration MR systems mitigating patient claustrophobia and body habitus issues. Contrast agents have increased the potential applications of MRI and helped to realize Damadian's contention that the modality could distinguish between neoplastic and nonneoplastic tissue.

Abdominal and gastrointestinal applications of MRI date back decades and continue to expand in scope to the present. In 1980, Edelstein et al reported one of the first examples documenting the acquisition of abdominal MR images using a "whole-body" magnet as a form of feasibility exercise [5]. Doyle et al. [6] reported one of the first series of cases of liver MRI studies, comparing them to computed tomography (CT) and concluded that "the information revealed is fundamentally different and can be expected to have some diagnostic utility." At the same time, MR contrast agents were being investigated; Young et al. [7] observed that following oral ingestion of a paramagnetic ferric chloride contrast agent (with similar properties to the gadolinium-based contrast agents administered today), "spin-lattice relaxation time can be altered in vivo…" meaning that relaxation is facilitated, with consequent hyperintensity of T1-weighted images,[1] enhancing contrast. While further work substantiated the utility of contrast enhancement using gadolinium-based contrast agents in the brain, early abdominal applications focused on T1- and T2-weighted image signal intensities in order to discriminate between different tissues [8]. For example, Stark et al. [9] showed that signal intensities on T2-weighted images were useful to distinguish hemangiomas from malignancy and concluded "T2-weighted spin echo (SE) imaging may become the procedure of choice for diagnosing cavernous hemangioma from liver cancer." Please see the following section entitled "MRI techniques" for further explanation of T1 and T2 weighting and diffusion images.

Shortly thereafter, the potential benefit of gadolinium contrast agent enhancement gradually becomes evident; Edelman et al. [10] concluded "…enhancement with Gd-DTPA [diethylenetriamine pentaacetate] is a practical method for improving liver-lesion contrast and has the potential to improve the accuracy of MR imaging in the liver." By the early 1990s, there was mounting evidence of the potential utility of contrast enhancement for abdominal applications. Semelka et al. [11] demonstrated the superiority of postcontrast MR images compared with CT and T2-weighted MR images. In the ensuing years, Gd contrast enhancement became engrained as a core component of not only liver examinations, but of all abdominal examinations.

Additional diagnostic tools have been developed, such as chemical shift imaging, diffusion-weighted imaging, elastography, and others that have had substantial impact on the practice of gastroenterology. Chemical shift (or in- and out-of-phase imaging) provides a semiquantitative assessment of hepatic steatosis and iron deposition in conjunction with other quantitative techniques that will be discussed in detail. Diffusion-weighted imaging serves as an adjunctive means of identifying neoplastic tissue, response to treatment, and other functions. Elastography offers a noninvasive alternative to tissue sampling in order to quantify fibrosis and help manage chronic liver disease (Fig. 2). Magnetic resonance cholangiopancreatography (MRCP) techniques have evolved over the decades to the point that MRCP is now an accepted alternative or adjunct to conventional endoscopic retrograde cholangiopancreatography (ERCP). MRI has also become

[1] T1- and T2-weighted imaging in MRI refers to two different strategies that exploit the unique behavior of different proton species reacting to electromagnetic energy, or radiofrequency pulses, in a strong magnetic field. T1-weighting is accomplished by repeating radiofrequency pulses either very rapidly and/or with high intensity to selectively isolate those protons that rapidly realign their nuclear spin with the main magnetic field (defined as having a low T1 value, which refers to the time elapsed for a proton to achieve 63% realignment with the main magnetic field). T1-weighting favors signal from protons with short T1 values, such as gadolinium and methemoglobin (blood). T2-weighting is accomplished by prolonging the acquisition of data, or the reception of the emitted radiofrequency energy from protons following an radiofrequency pulse to selectively isolate the received signal from proton species retaining relatively greater transverse, or coherent, magnetization as a function of their proton-specific T2 value (which is the time elapsed for 63% of transverse magnetization to decay following excitation by a radiofrequency energy pulse). T2-weighting favors signal from protons with long T2 values, such as water protons.

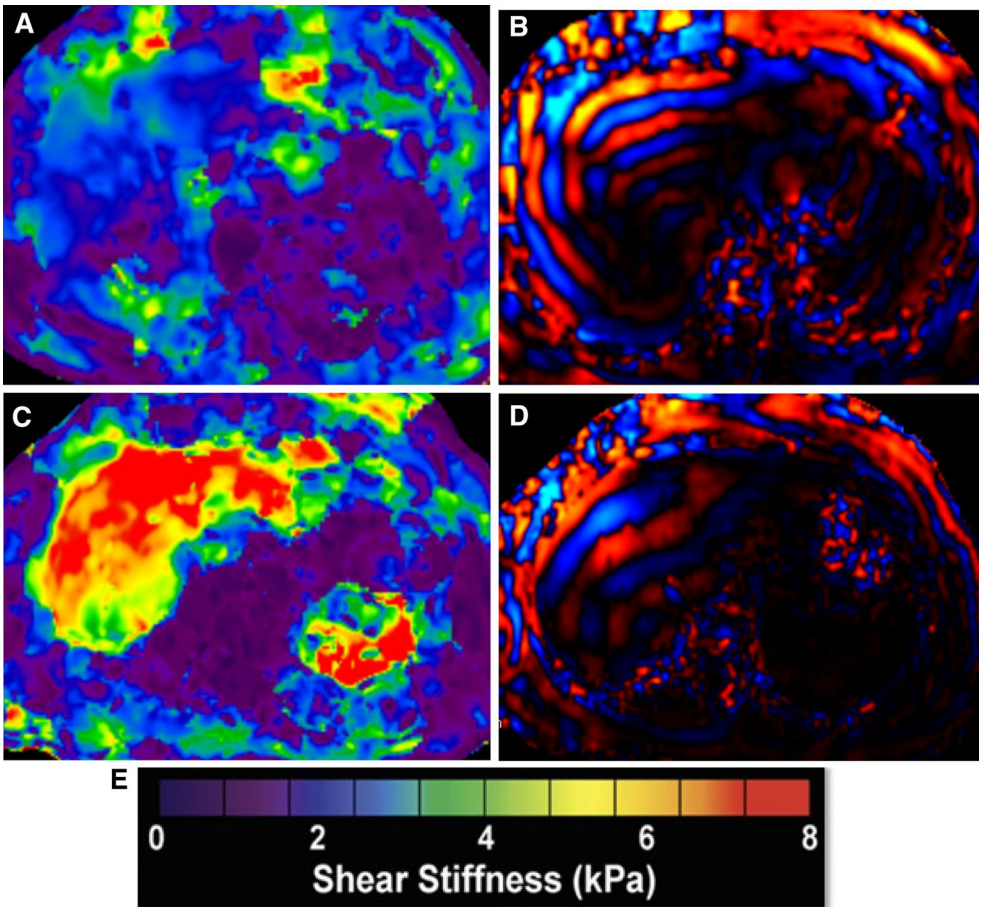

Fig. 2 MR elastography of the liver. Wave image (**a**) and color image (**b**) from an MR elastogram in a patient with normal liver stiffness show relatively low levels of stiffness reflected by the blue color in **a** and coherent color-encoded concentric waves in B. Conversely, the wave image (**c**) and color image (**d**) in a patient with stage 4 fibrosis, or cirrhosis, show high levels of stiffness depicted in red and less coherent wave propagation, respectively. Note the shear stiffness color scale (**e**) for reference

Fig. 3 GI applications of MRI

Liver	Biliary	Pancreas	Small Bowel	Large Bowel
Focal lesion characterization	Choledocholithiasis	Focal lesion characterization	Inflammatory bowel disease	Rectal cancer staging
Metastatic workup	Biliary dilatation etiology	Assessment of pancreatitis	Other inflammatory etiologies	Appendicitis evaluation
Fibrosis staging	Sclerosing cholangitis assessment		Polyposis syndromes	
Fat and iron quantification	Pyogenic cholangitis diagnosis		Celiac disease	
Response to percutaneous treatment		Etiology of pancreatitis	Small bowel tumors	Perianal fistula

the imaging "gold standard" for the diagnosis of pancreatic disorders because of its exquisitely high tissue contrast and multiparametric diagnostic capabilities. Additionally, MR system hardware improvements have shortened imaging times, with consequent improvements in the capability to image the gastrointestinal tract and perform MR enterography in conjunction with the development of oral contrast agents.

In today's world, MRI substantially contributes to multiple aspects of gastroenterological practice (Fig. 3). Among its numerous GI-related applications, MRI is the study of choice to evaluate focal liver lesions, serves as a noninvasive alternative to liver biopsy for the diagnosis of diffuse or infiltrative pathologic conditions, is the noninvasive "gold standard" for the evaluation of the biliary tree, is used to evaluate focal pancreatic lesions and pancreatitis and its complications, is a robust means of evaluating the small bowel in the context of inflammatory bowel disease and other conditions, is an alternative to CT and diagnostic

ultrasound (US) in the diagnosis of appendicitis, and is an accurate means of staging rectal carcinoma.

Technological improvements have enhanced the importance of MRI in these instances, such as faster imaging to accommodate breath holding and shorter and wider gantries that maximize patient comfort. While the expansion of clinical capabilities and applications in MRI in the field of gastroenterology has been impressive, the pace of innovation is unlikely to slacken, with ongoing work in areas such as combined positron emission tomography (PET)/MRI; bringing ultra-high-field MRI (7 T) to the forefront; and in exploring the feasibility of esophageal, gastric, and colonic imaging and others.

MRI Techniques

Tissue Contrast and T1WI, T2WI, and DWI

A typical abdominal MRI examination includes a variety of images called "pulse sequences." Each pulse sequence provides specific information about structures in the abdomen. Commonly used pulse sequences in abdominal imaging include "T1-weighted images," "T2-weighted images," and "diffusion-weighted images." T1-weighted images evaluate for fat, iron, protein, and blood [12, 13]. T1-weighted images are also used to perform gadolinium-enhanced MRI. T2-weighted images evaluate for fluid and edema and help differentiate solid from cystic lesions [14, 15]. Magnetic resonance cholangiopancreatography (MRCP) images, which are strongly T2-weighted, are designed to selectively isolate fluid from bile and pancreatic ductular tissue [16]. Diffusion-weighted images evaluate for dense cellularity (i.e., solid lesions) and tense edema (i.e., abscesses or inflammation) [17–19].

In addition to the tissue contrast provided by standard noncontrast MRI pulse sequences, T1-weighted images obtained after administering intravenous gadolinium provide additional tissue characterization information, which when combined with other pulse sequences leads to a specific tissue diagnosis in many cases [18]. The administered gadolinium highlights organs, vascular structures, and abnormalities, while the timing of enhancement provides additional temporal information. Specifically, early enhancement occurs with vascular structures or neoplasms, slow/progressive enhancement can indicate fibrosis or edema, and cysts or areas of necrosis will have no enhancement [18].

Further accentuating the clinical utility of gadolinium-enhanced MRI is the availability of 3 distinct categories of gadolinium-based contrast agents that can be used for abdominal MRI examinations [18, 20, 21]. This includes extracellular space contrast agents (ECSAs), hepatocyte-specific contrast agents (HSCAs), and blood pool agents (BPAs). The category selected depends on the indication for the examination. ECSAs are the "workhorse" category used for most abdominal indications such as abdominal pain or mass, cirrhosis evaluation to rule out hepatocellular carcinoma, or pancreas, kidney, adrenal, or spleen evaluation [22]. HSCAs are the agent of choice to exclude liver metastases, characterize focal nodular hyperplasia, and for bile duct evaluation such as excluding a bile leak [23, 24]. BPAs are mainly for vascular applications including MR angiography and MR venography [18, 25, 26].

GI Applications and the Value/Impact on the Practice of Gastroenterology

Accurate diagnostic imaging of the GI tract is necessary for the evaluation and treatment of GI and liver diseases. Over the past 20 years, advances in cross-sectional imaging with MRI have extensively changed GI imaging due to its major advantages when compared to traditional radiographic examinations [27]. In GI practice, MRI can be used for lesion characterization or as a problem-solving examination in cases in which the results from multidetector CT or US examinations are inconclusive or incomplete. Of the available modalities, MRI provides the most accurate detection and characterization of hepatobiliary disease and can be used for sophisticated assessment of benign and malignant hepatic tumors [28] attributable to the superior intrinsic properties of MR imaging in evaluating soft tissue contrast in comparison with CT. This difference may be important for detecting subtle areas of pathology and may improve characterization of certain abnormalities, such as in the evaluation of perianal fistulas in the setting of Crohn's disease. The MR imaging appearance of this condition shows greater concordance with surgical findings than any other imaging evaluation. Thus, MR has the potential to evaluate small and large bowel and perianal disease using a single imaging modality. The excellent inherent soft tissue contrast of MRI can be further improved by using gadolinium-based contrast agents including extracellular space contrast agents and liver-specific contrast agents [20, 21, 23].

With the increasing awareness of the short- and long-term hazards of radiation exposure, global interest has increased in implementing techniques that either reduce or eliminate radiation exposure [29]. This may be of particular importance in patients with chronic inflammatory bowel and liver disease, who may require multiple studies over a lifetime [30]. As a result, MRI has become increasingly important as a method of evaluating GI diseases [31, 32]. MRI combines the advantages of excellent soft tissue contrast, noninvasiveness, functional information, and lack of ionizing radiation [33], enabling gastroenterologists to have an increased level of confidence in their decision to pursue medical or surgical

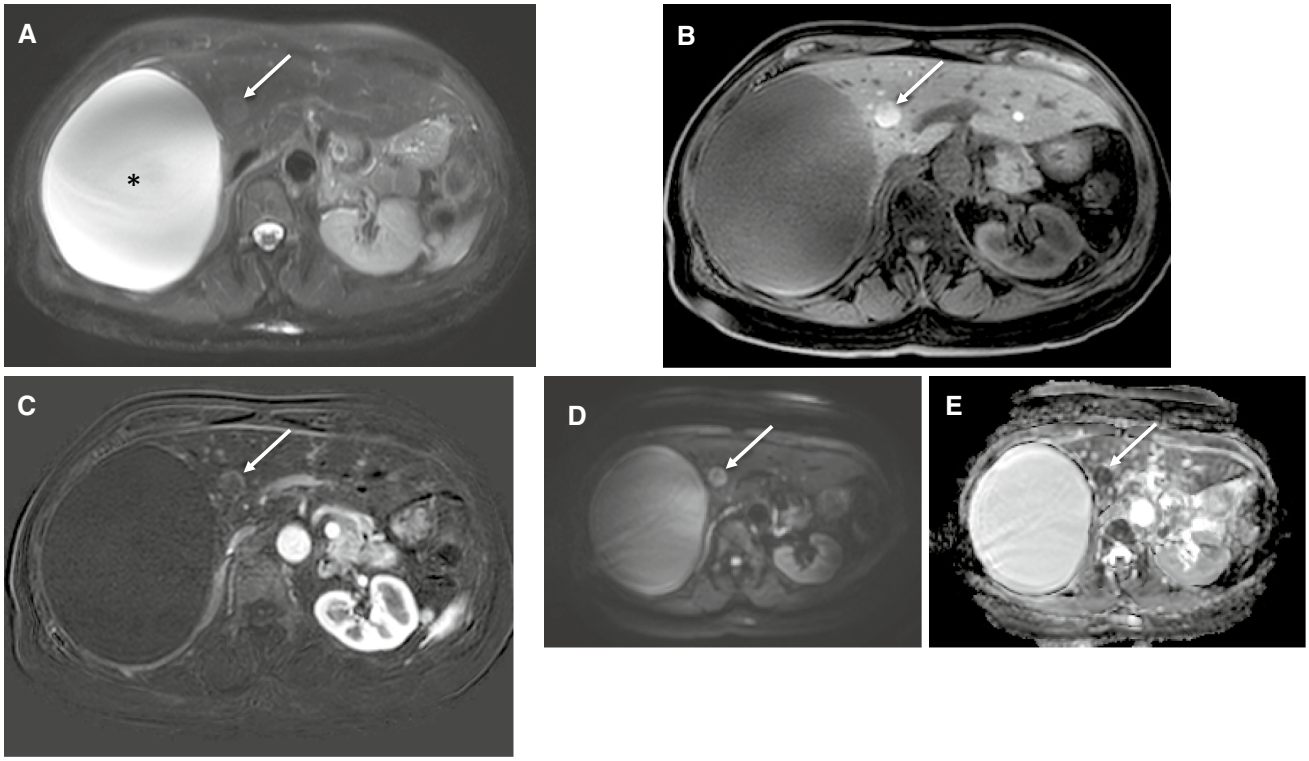

Fig. 4 Hepatic cyst compared with metastasis. The axial fat-suppressed T2-weighted image **a** shows the stark difference between the markedly hyperintense free water in the large simple cyst in the right lobe (asterisk) compared with the mild hyperintensity of the bound water in the adjacent ocular melanoma metastasis (arrow). On the corresponding fat-suppressed T1-weighted image (**b**), the cyst is hypointense and the metastasis is hyperintense because of its melanotic content. The postcontrast subtracted (arterial phase postcontrast minus precontrast) image **c** reflects the lack of enhancement in the cyst compared with the metastasis, which enhances (even following chemoembolization) indicating the presence of solid, viable tissue. The diffusion-weighted image **d** demonstrates a combination of T2 signal and diffusion restriction with nearly equal signal intensity between the cyst and metastasis. Signal intensity on the ADC map image **e** is directly proportional to diffusion and shows the stark difference between free water (cyst) and solid tissue (metastasis)

interventions [34]. The main drawbacks may be related to economic constraints and the need for subspecialized radiologists.

Hepatobiliary System

Liver

Liver Lesions

MRI can image virtually every GI structure, including the liver, biliary system and gallbladder, pancreas, spleen, small bowel, appendix, and rectum. Identifying and characterizing liver lesions was the first recognized GI application of MRI and has been the most widely utilized. By 1985, the exquisite tissue contrast properties of MRI were being realized as researchers demonstrated the value of T2-weighted imaging. Stark et al. [9] reported that T2-weighted images "may become the procedure of choice for distinguishing cavernous hemangioma from liver cancer" based on their comparison of cysts and hemangiomas with metastases. Subsequent work substantiated these findings, which are now deeply embedded into the MRI diagnostic armamentarium [35–37]. The physical principle behind this diagnostic tool is the difference in magnetization decay between free water protons (very prolonged) in the simple fluid contained in cysts and hemangiomas compared with that of bound water protons (much shorter) in solid tissue (Figs. 4 and 5).

The next major breakthrough in harnessing the diagnostic power of MRI was the introduction of contrast enhancement. While the T2 signal proved its ability to discriminate solid from cystic tissue using relative signal intensities, occasional overlap requires supporting techniques. Since intravenous contrast enhancement is delivered through the circulatory system, contrast enhancement effectively connotes solid tissue, which is necessarily vascularized (Fig. 4). This premise was substantiated by the early 1990s by numerous studies, including Semelka et al. [11], who in 1992 reported that contrast-enhanced MRI exceeded contrast-enhanced CT and T2-weighted MR imaging in differentiating between solid and cystic lesions and was "…particularly successful

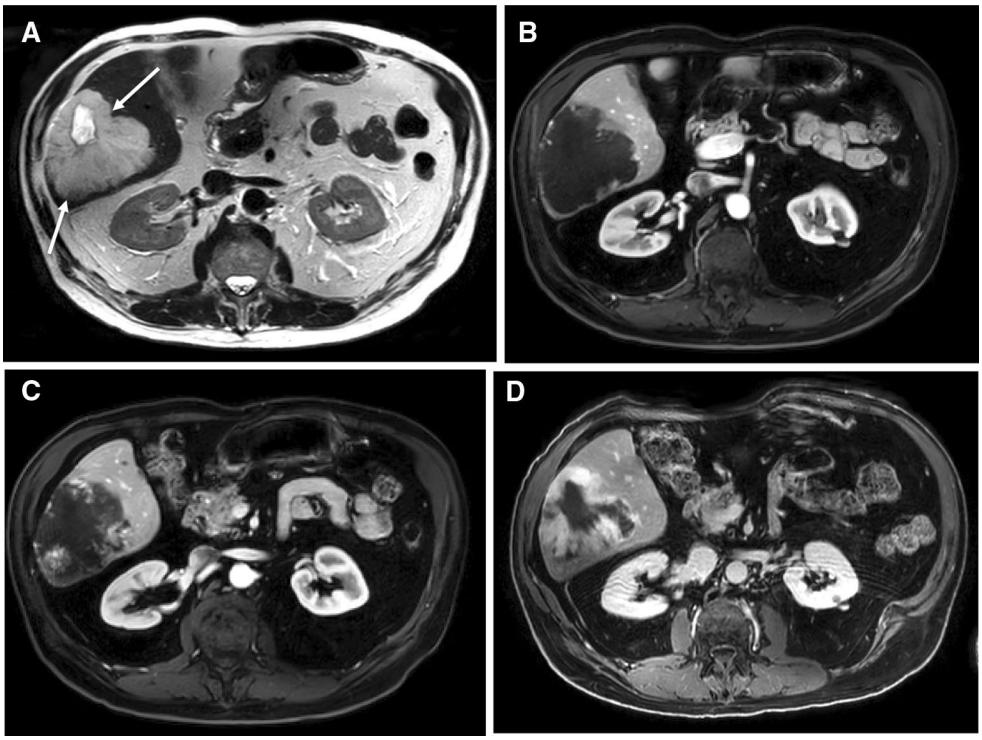

Fig. 5 MRI of liver hemangioma. The axial T2-weighted image **a** shows a giant hemangioma in hepatic segment 6 (arrows) with central cystic change contrasting with the less hyperintense periphery. Fat-suppressed T1-weighted postcontrast arterial phase (**b**), portal phase (**c**), and delayed (**d**) images demonstrate the classic clumped, discontinuous, and centripetally progressive hemangioma enhancement pattern that clinches the diagnosis

Fig.6 Liver lesion classification scheme

Cystic	Hypoenhancing	Hyperenhancing
Simple hepatic cyst	Hypovascular metastasis	Hypervascular metastasis
Biliary hamartoma	Cholangiocarcinoma	Hepatocellular carcinoma
Inflammatory lesions	Lymphoma	Focal nodular hyperplasia
Biliary cystadenoma (-adenocarcinoma)	Confluent fibrosis	Hepatocellular adenoma

in characterization of 5 mm to 1.5 cm diameter lesions as cystic or solid."

While discriminating the solid from cystic nature of liver lesions is an important first step in the diagnostic process, providing more specific diagnostic information is almost always necessary. Dynamic contrast enhancement—imaging before (precontrast) and then repetitively following intravenous contrast (postcontrast)—provides information beyond binary present or absent enhancement. Numerous studies have reported that the differential characteristics enhance hepatic lesions with relatively high specificity. For example, while technically fluid-filled, or "pseudocystic," hemangiomas exhibit a unique peripheral, clumped, discontinuous, and centripetally progressive enhancement pattern (Fig. 5), truly solid lesions enhance in a variety of patterns including rim enhancement of metastases and the hyperenhancement of hepatocellular carcinoma [38]. With the subsequent wealth of research on the MRI appearance of liver lesions, characterizing lesions based on enhancement is relatively straightforward. In conjunction with the appearance on T2-weighted imaging, the presence or absence of enhancement effectively addresses the question of solid versus cystic. When solid lesions are characterized as either hypoenhancing or hyperenhancing compared with the background liver (Figs. 6 and 7), numerous additional enhancement features help further characterize these lesions. For example, hepatocellular carcinoma (HCC) exhibits a number of unique enhancement features, including corona enhancement (rim of fading hyperenhancement), capsule appearance (delayed peripheral enhancement), and mosaic architecture (multicompartmental appearance). While ancillary features help characterization, the basic tenet of malignant

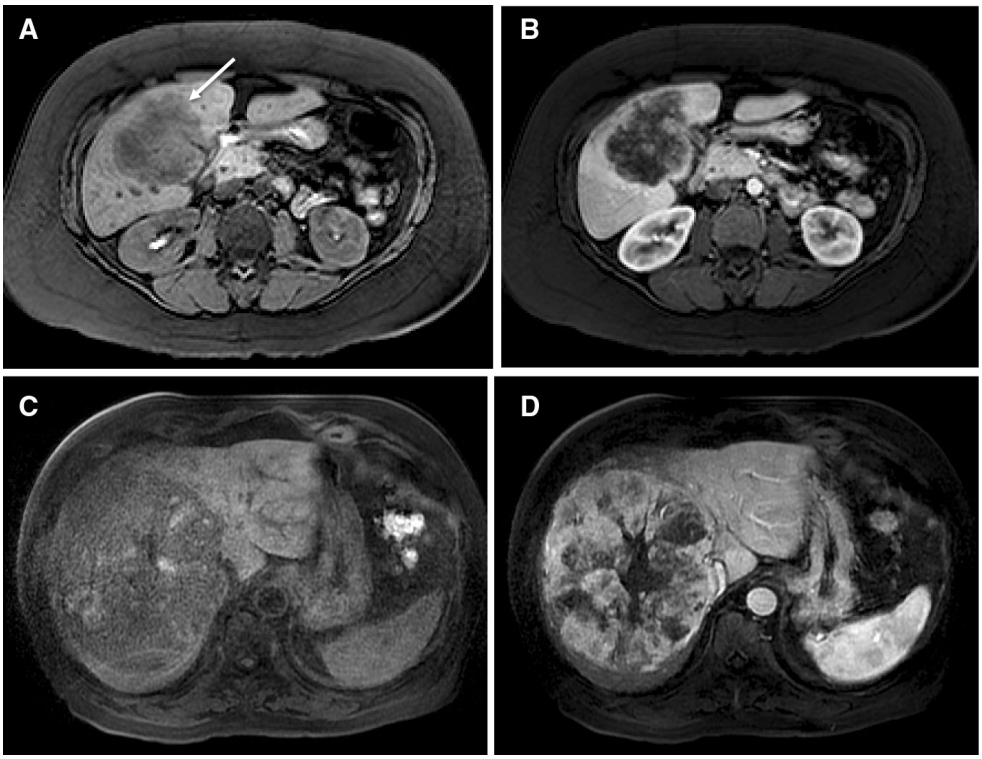

Fig. 7 Hypo- versus hyperenhancement. The axial fat-suppressed T1-weighted precontrast image **a** shows a hypointense liver lesion (arrow) representing a cholangiocarcinoma, which has minimal enhancement following contrast administration on the arterial phase postcontrast image (**b**). The axial fat-suppressed T1-weighted image in a different patient with hepatocellular carcinoma **c** shows a large right lobar lesion with foci of hyperintensity corresponding to hemorrhage. The arterial phase postcontrast image **d** shows mosaic architecture with hyperenhancement, typical of HCC

enhancement is washout, which means relative reduction in enhancement compared with the liver from an earlier to a later phase of enhancement appearing as portal and/or later phase hypoenhancement (in other words, the liver enhances relatively more over time compared with an HCC lesion causing it to become increasingly hypointense over time). Within the hyperenhancing category, benign lesions either fade to isointensity to liver (i.e., focal nodular hyperplasia and hepatocellular adenoma) or remain hyperintense (i.e., flash-filling hemangioma). Although hypoenhancing lesions, which are more protean, have enhancement kinetics that are more difficult to appreciate, the vast majority are hypovascular metastases. Less common hypoenhancing lesions demonstrate unique features including the peripheral and centripetally progressive enhancement of cholangiocarcinoma and the gradually progressive enhancement of confluent fibrosis.

The development of hepatocyte-specific MRI contrast agents (gadoxetate disodium or Eovist® or Primovist™) has added further diagnostic utility. In addition to providing similar dynamic enhancement information as standard extracellular contrast agents, gadoxetate disodium adds delayed hepatobiliary uptake, which helps to isolate nonhepatocellular lesions with high sensitivity (Fig. 8) [39–41]. Its secondary application is to establish the diagnosis of focal nodular hyperplasia (FNH), which hyperenhances and then retains contrast on delayed hepatobiliary phase imaging (Fig. 8) [42–44].

Diffusion-weighted imaging (DWI) confers additional diagnostic utility in detecting and diagnosing liver lesions. The unregulated growth in tumors translates to a relatively higher concentration of cell and cell membranes, which restrict water diffusion, and diffusion restriction is directly proportional to signal intensity on DWI. Because DWI is also T2-weighted, these images are effectively doubly weighted for malignant tissue, explaining the extreme sensitivity (Fig. 9).

The combination of these parameters explains the preeminent role of MRI in the evaluation liver lesions. Yet, despite this vast diagnostic armamentarium, data have failed to establish the diagnostic superiority of MRI over CT. A recent meta-analysis concluded that "no definitive recommendation can be made for systematic use of gadoxetate-enhanced MRI or extracellular contrast-enhanced MRI over CT [45]." While both modalities are reasonable liver-lesion imaging options, particular circumstances favor one over the other. In the case of large-volume ascites, (if not drained),

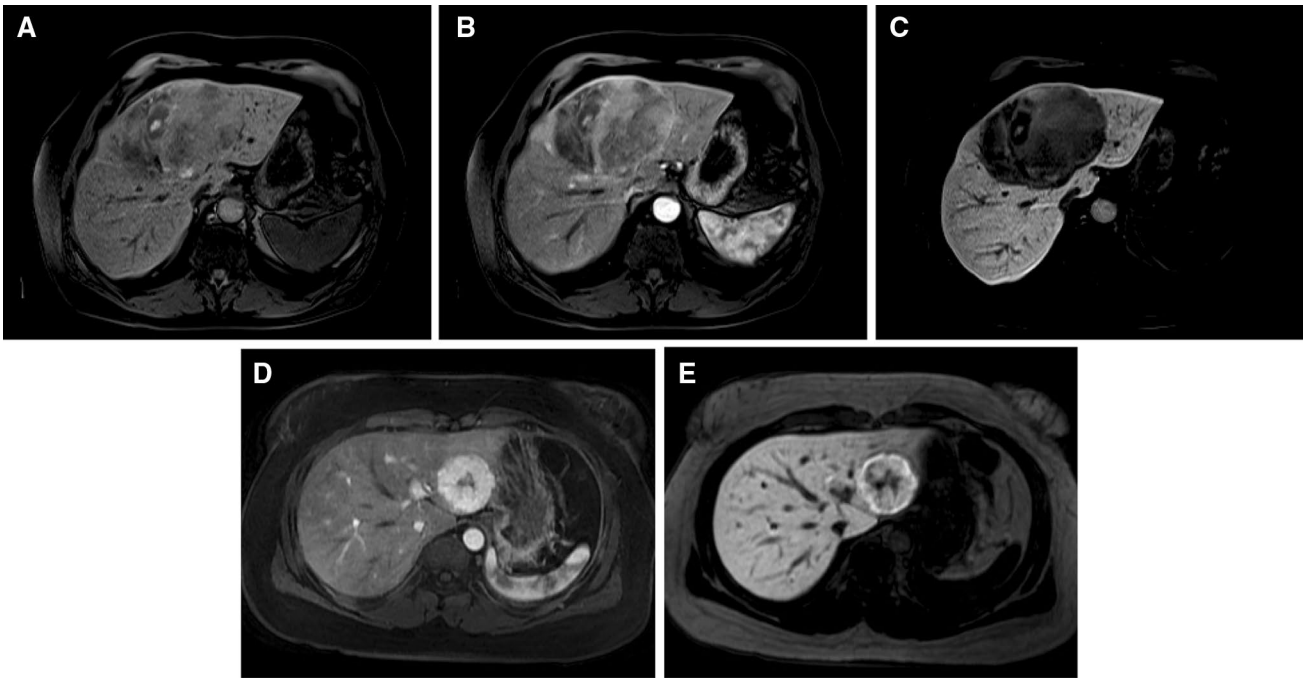

Fig. 8 Gadoxetate disodium enhancement. The fat-suppressed T1-weighted precontrast image **a** shows a mostly hypointense metastasis with hyperintense foci corresponding to hemorrhage. The postcontrast arterial phase image **b** shows hyperenhancement, typical of an ocular melanoma metastasis. The delayed hepatobiliary phase image **c** shows stark contrast between the hypointense metastasis (rendered slightly more hyperintense because of the superimposed hemorrhage) compared with the hyperintense normal liver parenchyma. Arterial phase postcontrast image **d** in a different patient shows an avidly hyperenhancing left lobar focal nodular hyperplasia (FNH) with a characteristic central scar. The corresponding delayed hepatobiliary phase image **e** shows persistent contrast hyperenhancement, which is diagnostic of an FNH

MRI potentially confronts the dielectric effect, especially on 3 T systems. Ascites presents a conductive medium in which a circulating electrical current is generated by the rapidly changing magnetic field. This current constitutes an electromagnet, which opposes the changing magnetic field and reduces the amplitude of the radiofrequency field and the subsequent signal contributing to image data. Breathholding limitations also favor CT over MRI, although recent innovations in MR image acquisition strategies have substantially shortened breathhold requirements [46]. In the setting of hepatocellular dysfunction, the poor uptake of gadoxetate disodium argues against the use of this agent.

Significance for Transplantation/Liver Imaging Reporting and Data System (LI-RADS)

Hepatocellular carcinoma (HCC) is the sixth most commonly diagnosed cancer worldwide [47], developing in the presence of cirrhosis in 90% of cases [48]. The 5-year cumulative incidence of HCC is 8–30% in patients diagnosed with cirrhosis [49]. The implementation of radiographic surveillance programs has enabled early tumor diagnosis increasing the probability of cure, achieving 5-year survival rates of up to 75% [50, 51]. In light of this survival benefit, the American Association for the Study of Liver Diseases (AASLD) recommends that HCC surveillance primarily consists of liver ultrasound at 6-month intervals [52]. According to the AASLD guidelines, when a nodule grows to $\geq$ 1 cm, MRI or CT is then recommended for surveillance. Because of its higher diagnostic accuracy for the detection and characterization of HCC, MRI has gained an increasingly predominant role in evaluating patients with chronic liver disease.

The therapeutic option of choice for HCC is liver transplantation (LT) since it removes both the neoplasm and any underlying cirrhosis. The most appropriate candidates for LT are patients that fit into the Milan criteria (single tumor $<$ 5 cm or up to 3 tumors of $<$ 3 cm) achieving a 5-year survival rate of 70%–80%. In these patients, the recurrence rates are ~ 10% [53, 54]. Based on this evidence, it is essential to be able to provide an accurate measurement of the size of an HCC and assess its potential for vascular invasion using diagnostic imaging such as MRI. To help with this assessment, LI-RADS was developed in 2011 in order to facilitate the interpretation and the reporting of CT and MRI examinations of the liver in patients at risk of HCC [55]. To address the limitations of prior assessment strategies, the development of LI-RADS had the goal of standardizing the

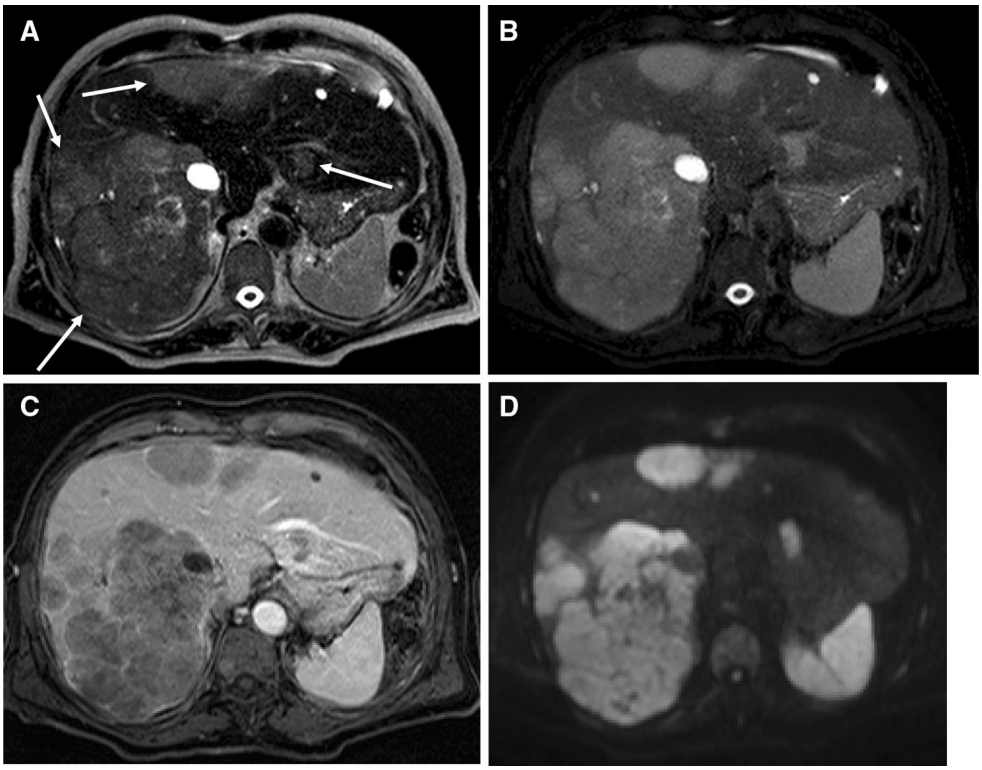

Fig. 9 Pulse sequences and tissue contrast. The axial T2-weighted sequence **a** shows mildly hyperintense masses corresponding to urothelial carcinoma metastases (arrows) and scattered hyperintense cysts. With fat suppression (**b**), the solid masses (arrows) are more conspicuous. The T1-weighted postcontrast image (**c**) demonstrates lesion hypoenhancement, which is typical of urothelial tumors. On the diffusion-weighted image (**d**), tissue contrast is extreme due to the combined differences in T2 signal and diffusion restriction between the metastases and the normal background liver

interpretation, reporting, and data collection of HCC imaging. Prior strategies generally categorized hepatic lesions as positive, negative, or indeterminate for HCC, with biopsy recommended for the latter. The problem was that for these strategies, the indeterminate category was very broad, including lesions that are likely to be benign and thus could safely be followed up without biopsy [56]. To address this, LI-RADS expanded the "indeterminate" category into probably benign, intermediate probability of HCC, and probably HCC (LI-RADS categories 2, 3, and 4, respectively), in order to facilitate personalized clinical decision-making. This system dovetails with the trend over the past two decades from the historic HCC diagnostic gold standard of tissue sampling toward relying on diagnostic imaging studies [57]. This trend reflects a combination of the risks of percutaneous biopsy and accuracy of diagnostic imaging studies. Biopsy risks include significant bleeding (2.5%) [58], death (0.06%) [59], 10–30% false-negative results [60–62] and up to 5% risk of tumor seeding along the biopsy tract [63–66]. Against this risk, the reliability of LI-RADS 1 and 2 classifications essentially guarantees benign etiology and justification for expectant management. A recent study reported that none of 122 LI-RADS 1 and LI-RADS 2 lesions (61 each) corresponded to a final diagnosis of HCC [67]. The same study found that 94% of 250 LI-RADS 5 lesions were correctly diagnosed and another study corroborated these findings by reporting a 97% positive predictive rate for 156 LI-RADS 5 lesions [68]. LI-RADS 3 and 4 lesions require an approach more customized to patient-specific factors. Both lesions generally benefit from a multi-disciplinary approach and are usually followed conservatively with follow-up imaging with biopsy in select cases [69]. Furthermore, LI-RADS is a dynamic strategy that will continue to be refined and updated as experience and validating data accrue [70].

As a bridge to liver transplantation and as a palliative therapy, there has been an evolution of minimally invasive, local-regional approaches to treat HCC lesions [71]. Regardless of the treatment modality, the best indicator of successful local-regional treatment is the absence of enhancement on postcontrast images [72]. MRI substantially contributes to the evaluation of the therapeutic response of HCC following the local-regional therapy. The treatment cavity occasionally appears T1 hyperintense in which case subtracted images better show the presence or absence of enhancement. Although a thin, smooth rim of hyperemic reactive tissue persists around the ablated cavity for several months,

nodular or mass-like internal or peri-lesional enhancement suggests residual or recurrent tumor.

Diffuse Liver Disease/Elastography

Chronic liver disease is a major cause of morbidity and mortality worldwide. The most common causes of chronic liver disease include hepatitis B, hepatitis C, nonalcoholic fatty liver disease, and alcoholic liver disease [73]. The importance of chronic liver disease is that it can progress to hepatic fibrosis and eventually cirrhosis. New data suggest that this is not an inexorable progression in that if fibrosis ensues, treatment can either slow, halt, or even reverse its progression. If cirrhosis develops, the imaging strategy changes to one focused on excluding hepatocellular carcinoma (HCC) and evaluating for portal hypertension [74, 75]. Currently, the "gold standard" for detecting liver fibrosis is percutaneous liver biopsy. Nonetheless, liver biopsy has significant limitations including patient reluctance, sampling error, heterogeneous fibrosis distribution, and inter-observer variability by pathologists reporting fibrosis of up to 20% [76, 77]. Liver biopsies can also be complicated by bleeding (1.7%) and death (0.2%) [74, 78]. Finally, monitoring response to treatment with liver biopsy is not ideal due to the above limitations.

MR elastography (MREL), a noninvasive imaging technique that evaluates for liver fibrosis, has revolutionized evaluation of patients with chronic liver disease [74, 75, 79]. With this technique, a plastic paddle placed on the abdominal wall generates vibrations that create "shear waves" in the liver which when measured can be quantitated (Fig. 2a). The speed that shear waves propagate through the liver is directly related to liver stiffness. Liver stiffness increases with increasing stages of liver fibrosis [80]. The ability to accurately stage the amount of fibrosis in the liver has made MREL an important diagnostic tool for patients with chronic liver disease. MREL can be used to detect or stage liver fibrosis, differentiate simple steatosis from nonalcoholic steatohepatitis, follow-up patients with chronic liver disease, and monitor treatment response [75].

Nonalcoholic Fatty Liver Disease (NAFLD)

NAFLD is defined as increased lipid (primarily triglycerides) accumulation in hepatocytes not associated with excessive alcohol use or other causes of fatty liver [81]. NAFLD is the most common cause of chronic liver disease in the USA, with a 30% prevalence. By 2020, NAFLD will likely be the most common etiology for advanced liver disease and indication for liver transplantation in the USA [82]. Patients with NAFLD can develop nonalcoholic steatohepatitis (NASH) with or without fibrosis. Long-standing NASH can progress to advanced fibrosis and eventually cirrhosis with its inherent complications including portal hypertension, liver failure, and HCC [83]. Standard imaging techniques using ultrasound, CT scan, and MRI only provide qualitative measurements of the amount of fat in the liver [84]. Nevertheless, a new MR technique creates a "fat fraction" map to quantify the triglyceride content in the liver [85–87]. This technique provides accurate quantitative liver fat measurements that in many cases may preempt a liver biopsy.

Hepatic Iron Overload

Hepatic iron overload can occur from increased intestinal iron absorption due to hereditary hemochromatosis (HH) or from repeated intravenous blood transfusions required to treat hematologic disorders such as thalassemia major, sickle cell disease, and myelodysplastic syndromes, or from advanced chronic kidney disease [88]. Quantifying the amount of iron in the liver is important in hemochromatosis patients as it may identify which patients need phlebotomy and helps to exclude disease with those at risk of developing HH based on genetic studies. For patients with iron overload, typically those receiving multiple blood transfusions, with hematologic disorders, or with severe kidney disease, the liver stores excess iron (up to 70% of the total body iron), which over time can lead to cirrhosis and HCC [89]. Quantifying hepatic iron in a liver biopsy is sometimes needed since blood tests such as transferrin saturation and ferritin are not always reliable. Hence, quantifying the amount of liver iron can help determine when chelation treatment is needed [88]. With MRI, a new technique can create an "R2*" map of the liver to quantify the amount of iron in the liver and to determine whether clinically significant iron overload is present, a method that may eventually replace the liver biopsy.

MRI Virtual Liver Biopsy

MR elastography, liver fat quantification, and liver iron quantification are usually performed at the same time to provide an MRI "Virtual Liver Biopsy" in less than 5 min. These techniques are generally combined with a standard gadolinium-enhanced abdominal MRI examination in order to provide the most comprehensive liver imaging available.

Biliary System

MRI is well adapted to the biliary system due to its ability to isolate bile from surrounding tissues. T2-weighted imaging favors signal from protons that retain energy longer after experiencing a radiofrequency energy pulse longer is usual, such as free water protons in fluid, which retain energy orders of magnitude longer than other proton species. This phenomenon becomes increasingly evident as the

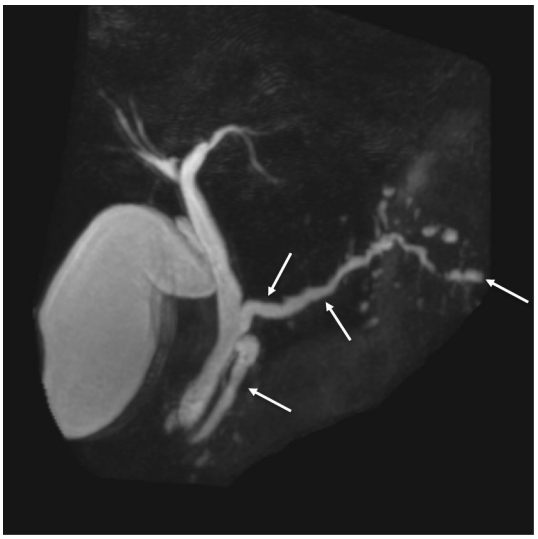

Fig. 10 MRCP isolating free water protons. The maximal intensity projection (MIP) image from a 3-dimensional MRCP isolates fluid from surrounding tissues and optimizes the characterization of ductal structures, such as the irregularly dilated pancreatic duct (arrows) with ectatic sidebranches in this patient with chronic pancreatitis

imaging time, or TE (or time to echo), is increased to the point where only fluid maintains energy or signal. These images containing signal from free water protons alone can be targeted to the biliary system, in which case they are called magnetic resonance cholangiopancreatographic (MRCP) images (Fig. 10). MRCP, first described in 1991, rapidly demonstrated its ability to accurately image the biliary system [90], whereas its diagnostic sensitivity and specificity do not quite match those for endoscopic retrograde cholangiopancreatography (ERCP)—reported as high as 93 and 99%, respectively [91]—its noninvasive nature, lack of contrast administration, lack of substantial risk, and opportunity to evaluate structures outside the biliary tract render it a very useful diagnostic modality. Since its inception in 1991, the MRCP pulse sequence armamentarium has expanded from a single heavily T2-weighted pulse sequence to updated programs including numerous additional pulse sequence options (Fig. 11). While the conventional notion of an MRCP includes only noncontrast T2-weighted pulse sequences (2-dimensional and 3-dimensional, if technical capabilities permit), contrast-enhanced MRCP techniques are also useful. For over two decades, MRCP has been accepted as the noninvasive diagnostic "gold standard" for biliary diseases. Guibaud et al. [92] demonstrated the diagnostic superiority of MRCP for the diagnosis of choledocholithiasis compared with ultrasound and CT, and Boraschi et al. [93] substantiated these results in nearly 300 patients by reporting a sensitivity of 93%, specificity of 98%, a positive predictive value of 92%, a negative predictive value of 98%, and an accuracy of 96%. MRCP has also been reported to have similar performance characteristics in the assessment of anatomic anomalies such as variant cystic duct anatomy and aberrant right hepatic ducts, postsurgical complications, inflammatory disease such as sclerosing cholangitis and malignant ductal obstruction (Fig. 12) [94].

The advent of hepatobiliary contrast agent usage has enhanced the capabilities of MRCP. Although gadoxetate disodium-enhanced images supplement the information provided by standard T2-weighted MRCP images for most diagnostic applications, they have been adopted as the primary means of identifying bile leaks. Extrabiliary contrast identifies sites of bile duct injury and bile extravasation and accumulation within bilomas. Due to its diagnostic utility in this regard combined with the ability to depict anatomic detail and other conditions, MRI/MRCP offers a compelling alternative to hepatobiliary scintigraphy in the setting of bile duct injury and biloma. The plethora of diagnostically accurate MRCP techniques explains its primary contribution to the evaluation of biliary diseases over other diagnostic imaging modalities and even in place of ERCP, in some instances.

Fig. 11 MRCP pulse sequences

Pulse Sequence	T1/T2	Contrast	Details
Single-shot	T2	No	Anatomic images with fluid contrast
Radial slab	T2	No	Radial slices isolating fluid-filled structures targeted to biliary and pancreatic ducts
3-D MRCP	T2	No	Respiratory triggered coronal volume isolating fluid-filled structures covering biliary and pancreatic ducts
Enhanced	T1	Gadoxetate disodium	Hyperintense contrast excreted into the biliary system after 20 minutes
*Delayed postcontrast T1-weighted images using standard extracellular contrast agents also provide detailed anatomic depiction of hypointense biliary radicles against hyperintense liver parenchyma.			

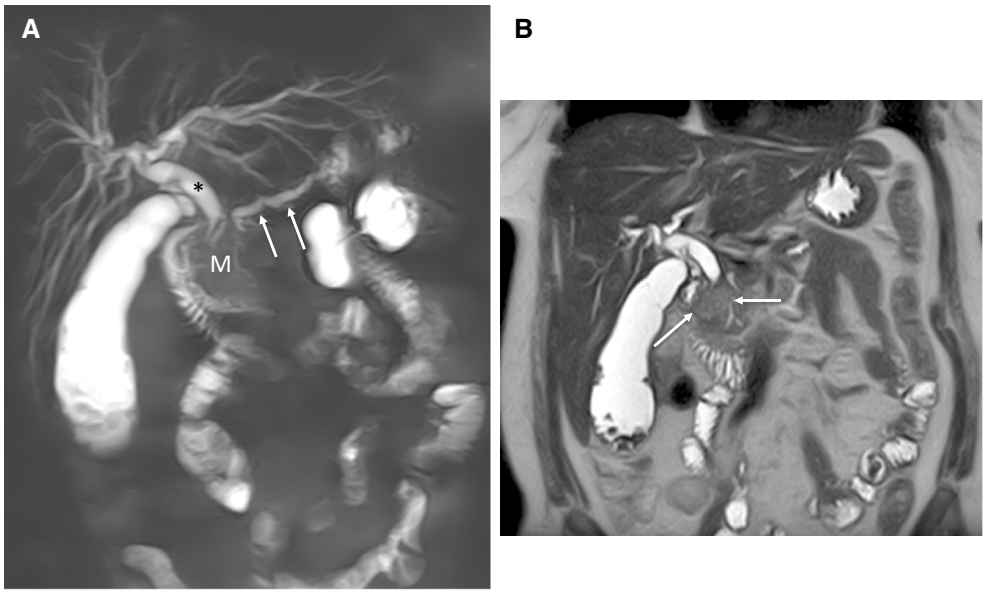

Fig. 12 MRCP image showing the "double-duct" sign. The MRCP image **a** shows the dilated common bile duct (asterisk) and biliary tree and the dilated pancreatic duct (arrows) converging on a pancreatic head mass (M), which is not visible on this pulse sequence. Filling defects in the gallbladder represent gallstones. The corresponding coronal T2-weighted image **b** shows the pancreatic head mass (arrows), but only partially demonstrates biliary and pancreatic ductal dilatation

Pancreas

Solid Masses

The predominance of MR imaging of the pancreas occurred after MR was considered to be the superior modality for imaging of the liver and biliary system. In their review of the status of MRI, Margulis and Fisher [95] concluded "it appears that without addition of contrast media, MRI offers no advantages over the CT and US." By the beginning of the next decade, the feasibility and utility of contrast enhancement for pancreatic disease were being realized. Chezmar et al. [96] suggested that pancreatic enhancement "has the potential to improve visualization of pancreatic masses." Semelka et al. [97] explained the utility of MRI in evaluating various pancreatic disorders from acute and chronic pancreatitis to focal lesions, such as ductal adenocarcinoma, periampullary masses, islet cell tumors, and cystic lesions. This utility arises in part because of the inherent attributes of the pancreas, attributable to its endocrine and synthetic properties. The normal pancreas exhibits hyperintensity on T1-weighted images and markedly avid arterial enhancement, both of which render virtually all lesions relatively hypointense. Furthermore, the fluid within the pancreatic duct and cystic lesions is markedly hyperintense against the relatively hypointense background normal pancreatic parenchyma, enabling ready detection and characterization, which is supplemented by contrast enhancement.

Whereas CT is the dominant imaging modality used in the evaluation of pancreatic adenocarcinoma, the multiplicity of pulse sequences with different tissue contrast properties and the sensitivity of diffusion-weighted imaging generally exceed the capability of CT in detecting small or infiltrating masses and metastatic spread (Fig. 13). Since pancreatic adenocarcinoma is T1-hypointense and hypovascular due to its neoplastic nature and desmoplastic content, it is particularly conspicuous against the T1-hyperintense, hypervascular pancreatic parenchyma. Nevertheless, the literature regarding the use of current, 3-D dynamic contrast MR imaging for pancreatic adenocarcinoma is limited. Notwithstanding, MRI has gained importance in the imaging evaluation of pancreatic adenocarcinoma due to its superior sensitivity for liver metastases, as previously discussed. Furthermore, MRI has a higher sensitivity to peritoneal and omental metastases, compared with CT [98].

Cystic Lesions

Advances and improvements in imaging technology have set off a virtual explosion of newly diagnosed pancreatic cystic lesions. The efficacy of MRI in evaluating pancreatic cystic lesions is unchallenged; due to its exquisite tissue contrast, MRI surpasses other imaging modalities in the ability to fulfill the three chief functions of pancreatic cystic lesion evaluation: 1) morphology, 2) relationship to the pancreatic duct, and 3) solid components (Fig. 14). MRI provides confident discrimination of benign serous

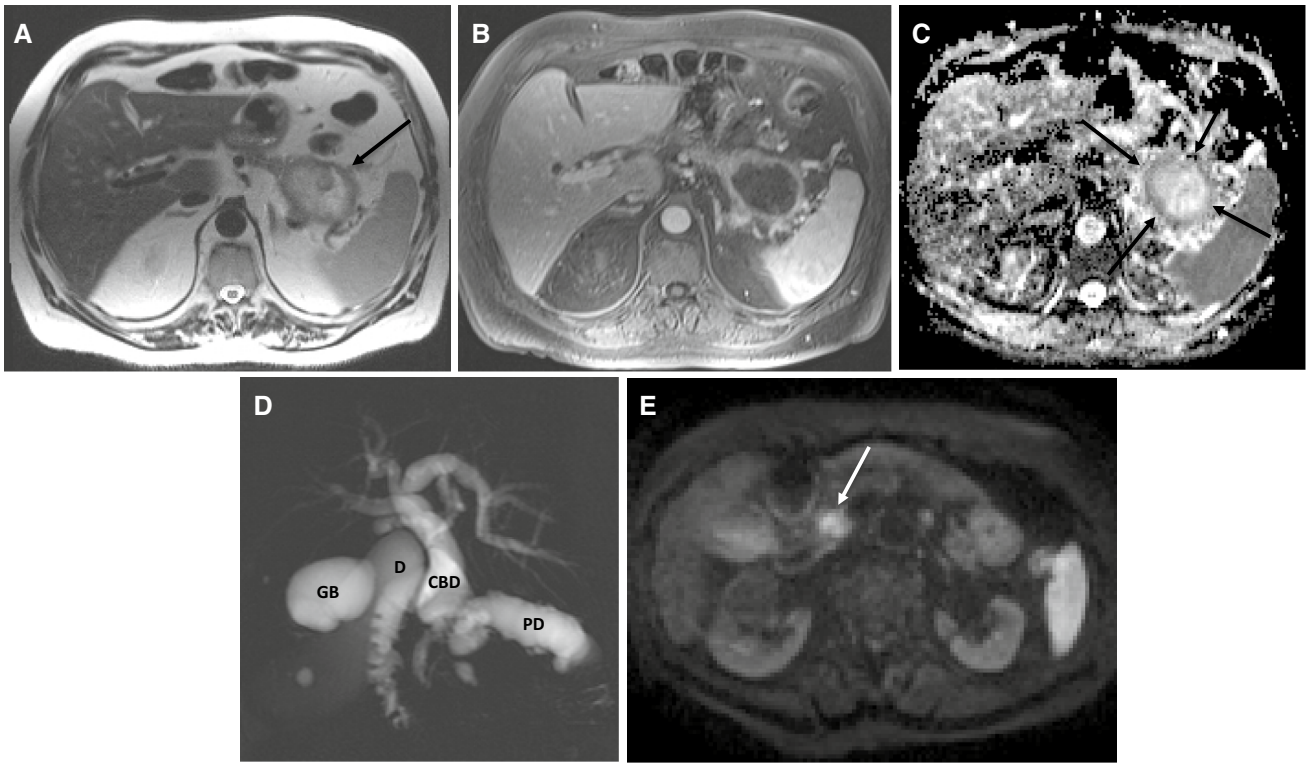

Fig. 13 MRI of pancreatic adenocarcinoma. The axial T2-weighted image **a** shows a large necrotic pancreatic tail mass (arrow). The corresponding axial fat-suppressed T1-weighted postcontrast image **b** confirms the lack of enhancement in the necrotic center with a rind of peripheral enhancing tissue. The ADC map image **c** shows the hypointense, diffusion-restricting peripheral viable tumor (arrows). The MRCP image **d** in a different patient exemplifies the double-duct sign with pancreatic and biliary ductal dilatation upstream from a pancreatic head mass (*GB* gallbladder, *D* duodenum, *CBD* common bile duct, *PD* pancreatic duct). The corresponding diffusion-weighted image **e** shows the hyperintense, diffusion-restricting mass in the pancreatic head (arrow)

cystadenomas from mucinous neoplasms, which are at least potentially malignant and require surveillance at the minimum. The distinctive features of lobulated margins and lack of communication with the pancreatic duct in the setting of an oligocystic or microcystic lesions (especially in the pancreatic head) uniquely characterize this lesion. Mucinous cystic neoplasms are typically oligocystic without lobulation and with convex margins almost always located in the distal pancreas. Intraductal papillary mucinous neoplasms (IPMNs) occasionally demonstrate a microcystic appearance, although more commonly conform to pleomorphic morphology and feature communication with the pancreatic duct by definition.

Fluid Collections and Pancreatitis

Although pancreatic fluid collections can also potentially simulate cystic neoplasms, the history of pancreatitis usually confirms their etiology. In addition to detecting pancreatic fluid collections, MRI also provides valuable information in the setting of pancreatitis. The inflammatory changes in acute pancreatitis are amply demonstrated, along with hemorrhagic change, necrosis, and vascular complications, findings usually equivocal when imaged using CT (Fig. 15). In chronic pancreatitis, MRI clearly demonstrates the parenchymal atrophy and fibrosis along with the characteristic irregular, dilated beaded ductal appearance. All imaging modalities occasionally struggle with differentiating the changes of chronic pancreatitis from pancreatic adenocarcinoma. In this setting, MRI has the highest likelihood of making this distinction with a sensitivity and specificity of 85 and 95%, respectively [99]. Differentiating acute interstitial edematous pancreatitis (and pancreatic adenocarcinoma) from autoimmune pancreatitis is also feasible with MRI; confirmation with elevated serum IgG4 concentrations can facilitate appropriate treatment with steroids. Pancreatic enlargement without peripancreatic inflammation with ductal attenuation and a distinctive hypointense surrounding capsule are the typical MRI findings.

Future of Pancreatic Imaging

Advances in MRI technology have improved the quality of pancreatic imaging, elevating it to an essential diagnostic

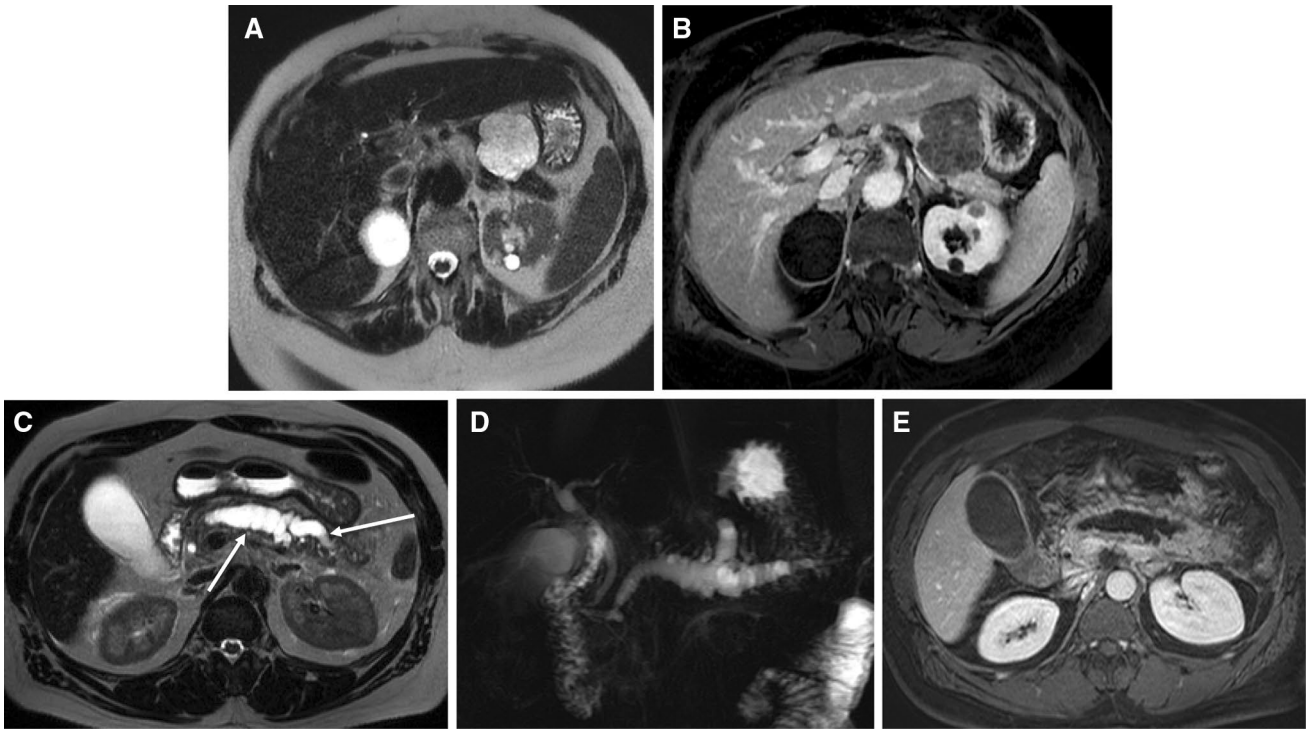

Fig. 14 MRI of pancreatic cystic lesions. The axial T2-weighted (**a**) and T1-weighted fat-suppressed (**b**) images in a 75-year-old woman reveals a lobulated and septated cystic lesion corresponding to a serous cystadenoma—no ductal communication was established on the MRCP images (not included). The axial T2-weighted image in a different patient with a main duct intraductal papillary mucinous neoplasm shows a tubular cystic lesion (arrows), which is seen to be fusiform dilatation of the pancreatic duct on the MRCP image (**b**). The corresponding T1-weighted fat-suppressed image **e** shows absent enhancement of the lesion compared with the surrounding enhancing pancreatic tissue

procedure. Future directions include diffusion-weighted imaging (DWI) to differentiate simple cysts from pseudocysts and neoplastic cysts, chronic pancreatitis from normal pancreas, and adenocarcinoma from pancreatitis. A variation of DWI, intravoxel incoherent motion (IVIM), also incorporates bulk flow information from capillary flow—or perfusion. Preliminary work suggests that perfusion information from IVIM will help discriminate hypoperfused adenocarcinomas from normal pancreatic tissue [100]. Finally, preliminary findings obtained from MR spectroscopy studies have indicated that pancreatic cancers harbor a higher level of lipid compared with pancreatitis [101].

Gastrointestinal Tract

Introduction

Given the universal availability of computed tomography (CT) and the obstacles provided in obtaining high-quality MRI examinations of the bowel, which include bowel peristalsis, respiratory motion, cardiovascular pulsations, and the lack of a suitable enteric contrast agent, the bowel was one of the last gastrointestinal organs evaluated with MRI. These obstacles have been overcome by the development of faster pulse sequences that have less motion artifact, the use of antiperistalsis agents to slow bowel motion, and the availability of several enteric contrast agents to highlight the bowel wall [102–105]. Because of these advances, MRI is now used to image a variety of GI conditions such as inflammatory bowel disease, bowel and mesenteric masses, celiac disease, rectal carcinoma, perianal fistulas, and appendicitis. With MRI, specific protocols have been designed to provide optimal images for each indication (Fig. 16).

While CT is a faster technique that is more readily available and has higher spatial resolution, MRI has significant advantages over CT, which makes MRI the imaging test of choice for many GI applications. For example, MRI avoids ionizing radiation, which can be important in patients with Crohn's disease or polyposis syndromes, many of which require multiple imaging studies starting at a young age [102]. Since the soft tissue contrast of MRI is superior to CT, MRI is more sensitive for identifying bowel wall edema or fibrosis and soft tissue masses. Furthermore, the inherent chemical properties of gadolinium result in superior tissue enhancement in comparison with CT iodinated agents, with

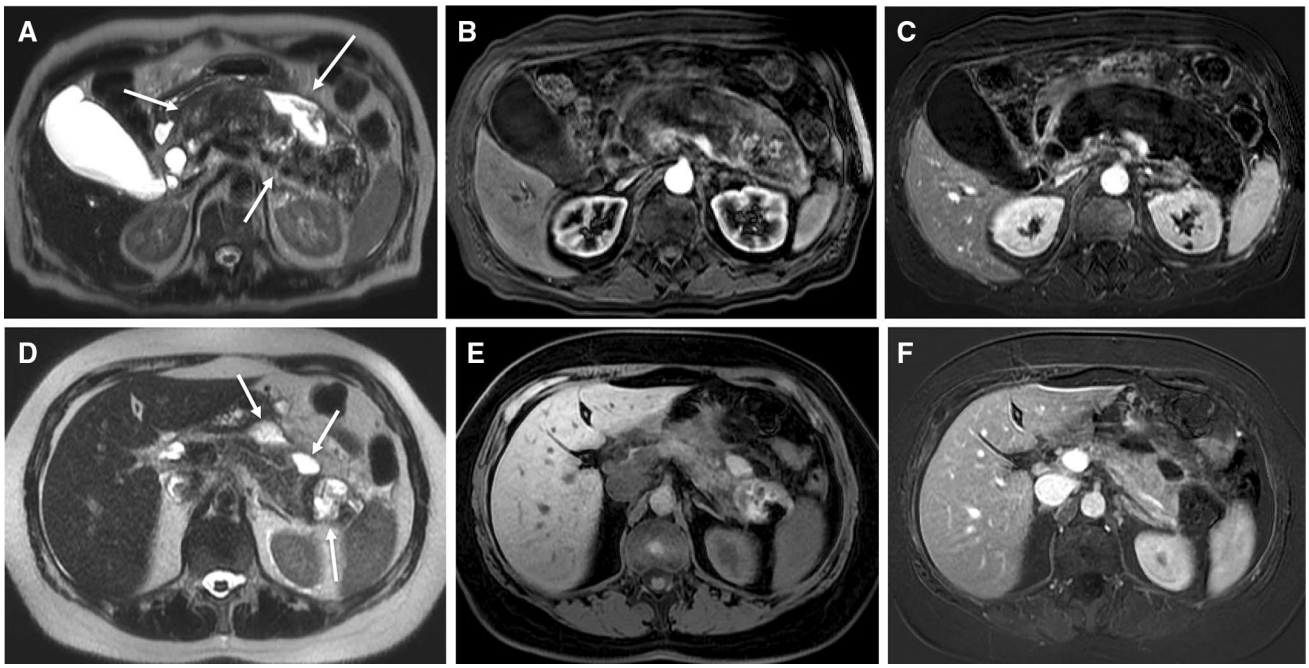

Fig. 15 Acute Pancreatitis. The axial T2-weighted image **a** shows a heterogeneously enlarged pancreas (arrows) in a patient with severe pancreatitis. The pancreas appears mostly hypointense with scattered hyperintensities on the T1-weighted fat-suppressed postcontrast image **b**. However, the subtracted image **c** reveals essentially no signal, or enhancement, indicating extensive necrosis and necrotizing pancreatitis. An axial T2-weighted image in a different patient week after the onset of acute interstitial edematous pancreatitis **d** shows mild pancreatic edematous hyperintensity with at least heterogeneous peripancreatic fluid collections (arrows), which are variably hyperintense on the precontrast fat-suppressed T1-weighted image **e** indicating hemorrhage. The subtracted image **f** confirms pancreatic enhancement, or tissue viability, and lack of enhancement in the pseudocysts

a better blood pool phase to obtain delayed images, while requiring a far lower dose of contrast compared to CT [106]. Furthermore, multiple dynamic contrast-enhanced phases can be obtained with MRI to evaluate the temporal enhancement of the bowel and soft tissues [18]. Finally, MRI can evaluate small bowel peristalsis by using a pulse sequence called "cine MRE" which creates a video depicting small bowel peristalsis [107]. This cine MRE can help identify abnormal small bowel segments, strictures, adhesions, and bowel masses.

MR Enterography (MRE)

The most commonly performed MRI protocol for the gut is MRE, which is an MR examination tailored for evaluating the small bowel. With MRE, patients drink up to 1.5 L of an oral solution designed to distend most of the small bowel and highlight bowel wall abnormalities. Gadolinium is administered to enhance the bowel wall, and antiperistalsis agents are usually given to decrease small bowel peristalsis. A variety of pulse sequences are performed providing thorough evaluation of the small bowel and adjacent structures. Cine sequences are included to evaluate small bowel peristalsis [108].

MRE is most commonly used to evaluate inflammatory bowel disease, especially Crohn's disease (CD). With CD, in more than 70% of patients, the small bowel is involved, which is the least accessible portion of the bowel by endoscopy [109]. In about 50% of CD patients, bowel involvement may skip the terminal ileum or involve the intramural or mesenteric distal ileum leading to negative ileocolonoscopy results [110]. When an acute CD flare occurs, the clinical presentation of active inflammatory Crohn's disease and potential complications such as abscess, fistula formation, or small bowel obstruction can be clinically indistinguishable. For these reasons, cross-sectional imaging with MRI and CT provides complementary information to ileocolonoscopy in CD patients [109, 111, 112]. In CD patients, MRE can readily identify active bowel inflammation, strictures, and penetrating complications such as fistulas, sinus tracts, and abscesses (Fig. 16). MRE can also evaluate for the presence of perianal fistulas and abscesses although if detailed evaluation is needed, high-resolution pelvic fistula MRI can be performed (discussed below). Finally, with MRE, extraintestinal complications of CD can be identified such as femoral head avascular necrosis, primary sclerosing cholangitis, sacroiliitis, and mesenteric venous thrombosis [113].

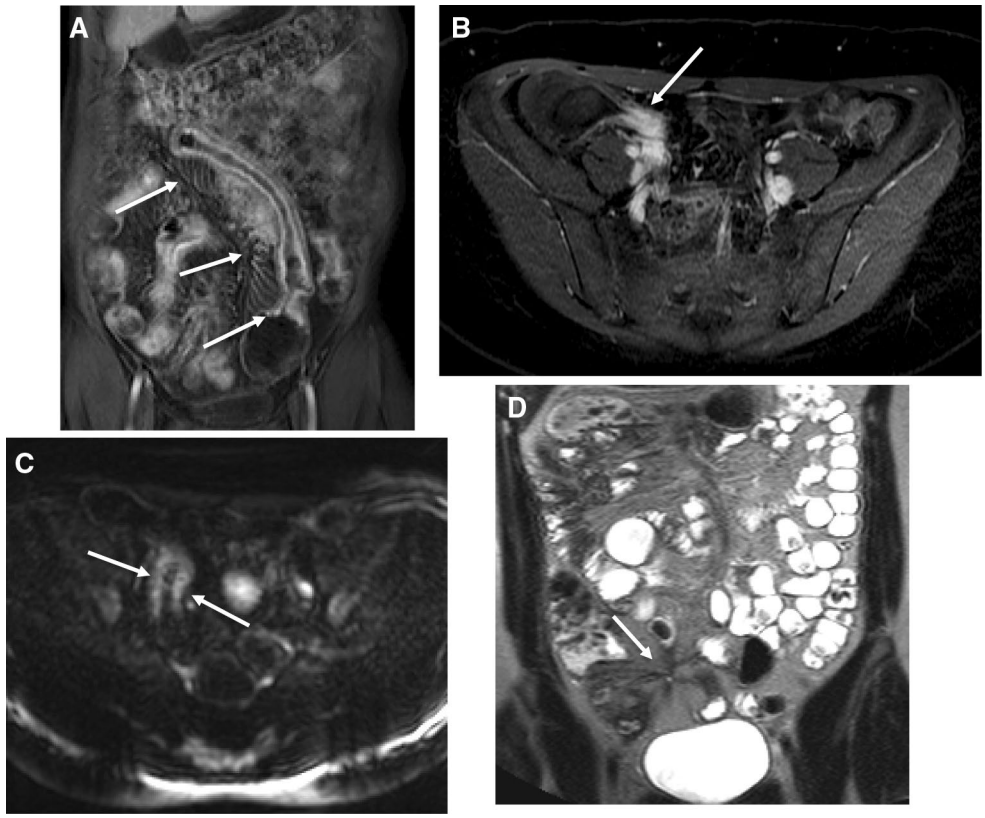

Fig. 16 MR enterography in inflammatory bowel disease. The coronal T1-weighted postcontrast image **a** shows mesenteric vascular congestion—the "comb sign" (arrows)—associated with a thick-walled, hyperemic, acutely inflamed loop of small bowel. Axial T1-weighted postcontrast image in a different patient **b** with active terminal ileal inflammation shows mural hyperemia (arrow); the corresponding diffusion-weighted image **c** reveals hyperintensity (arrows), indicating diffusion restriction arising from hypercellularity in the setting of Inflammation. The coronal T2-weighted image in a different patient **d** shows tethering between multiple bowel loops in the setting of penetrating disease and fistulization—the "star sign" (arrow)

Other Applications

Rectal Carcinoma Staging

MRI protocols can also be tailored for rectal carcinoma staging, perianal fistula evaluation, and to exclude the diagnosis of appendicitis. For rectal carcinoma staging, MRI can determine the location of the tumor relative to the anal verge, the depth of rectal wall invasion, the presence of peritoneal or adjacent organ invasion, and the presence of extramural vascular invasion. MRI can also evaluate for abnormal lymph nodes in the mesorectal fossa and along the pelvic sidewall. This information can guide colorectal surgeons in determining the need for chemoradiation or radiation therapy prior to surgery. For low rectal tumors, MRI can determine whether there is involvement of the internal anal sphincter tin order to determine whether sphincter-sparing surgery can be performed [114]. For patients treated with neoadjuvant chemoradiation or radiation therapy, MRI can determine the amount of residual tumor and the status of the circumferential resection margin to help plan treatment [115].

Perianal Fistula Evaluation

For perianal fistula evaluation, high-resolution pelvic fistula MRI has replaced previous imaging techniques such as fistulography, computed tomography, and endosonography [116, 117]. The multiplanar capability and excellent soft tissue contrast of MRI facilitates identification of perianal fistulas, the anal sphincter complex, and the relationship of the fistula to the levator plate and ischiorectal fossa. Accurate characterization of fistulas and possible abscesses helps guide appropriate surgical and medical treatment [116–118].

Appendicitis

While CT scanning is the test of choice in evaluating the appendix, for pregnant patients in which ionizing radiation should ideally be avoided, noncontrast MRI offers a viable

imaging option compared to CT [119]. With MRI, "edema-specific" pulse sequences and diffusion-weighted images help identify an abnormal appendix with high specificity and sensitivity [120]. Not only can MRI exclude appendicitis in these patients, but alternative diagnoses that may be causing symptoms can be identified such as acute pyelonephritis, obstructive uropathy, cholecystitis, placental abruption, a degenerating fibroid, or an ovarian cyst [120].

Conclusion and Future Directions

While the origins of MRI date back at least 135 years, its entry into the clinical world is less than four decades old and its impact on the practice of gastroenterology is three decades old. Early applications included liver lesion characterization and evaluating the biliary tree. With technological advancements, additional applications were realized, including pancreatic and rectal imaging, enterography, and elastography. Its multiparametric armamentarium—T1- and T2-weighted imaging, dynamic contrast enhancement, diffusion-weighted imaging, hepatobiliary phase imaging, and elastography—renders MRI an essential diagnostic tool in gastroenterology.

Given the central function of MRI in the practice of gastroenterology, it might seem there is little opportunity to augment its role. Yet, early work suggests that ultra-high-field MRI (7 T) has the potential to provide information regarding chronic liver diseases, such as NAFLD and cirrhosis. Magnetic resonance spectroscopy measuring ^{31}P metabolites, which includes cell membrane precursors (phosphomonoesters) and cell membrane degradation products (phosphodiesters), has been studied as a means to potentially diagnose, assess, and monitor the progression of NAFLD and cirrhosis [121–123]. Still, even on 3 T systems, this technique is time-consuming and diagnostically challenging since three additional ^{31}P metabolites are commonly encountered. At 3 T, discriminating the 5 ^{31}P substances, or spectroscopy peaks, is often not possible, but resolution improves proportionally with field strength, which enables peak separation at 7 T. The benefits of higher spatial resolution and greater signal-to-noise ratio with faster imaging promise to make this technique more clinically relevant [124]. Whether other novel applications will follow remains to be seen, but certainly seems compelling given the proven diagnostic superiority of MRI and its extremely high patient safety profile.

Compliance with ethical standards

Conflict of Interest Dr. Roth is an author for Elseiver and Dr. Halegoua-De Marzio receives grant/research support from Bristol-Myers Squibb, Conatus, Galectin, Genfit, Gilead, and Intercept and has been a consultant for Alexion, Gilead, and Intercept.

References

1. Indicators O. *Health at a Glance 2011. OECD Indicators*. Paris: OECD Publishing; 2015. https://doi.org/10.1787/health_glance-2015-en. **(Accessed February. 2015;15:2016)**.
2. Damadian R. Tumor detection by nuclear magnetic resonance. *Science*. 1971;171:1151–1153.
3. Lauterbur P. Image formation by induced local interactions: examples employing nuclear magnetic resonance. *Nature*. 1973;242:190–191.
4. Mansfield P. Multi-planar image formation using NMR spin echoes. *J Phys C Solid State Phys*. 1977;10:L55.
5. Edelstein WA, Hutchison JM, Johnson G, Redpath T. Spin warp NMR imaging and applications to human whole-body imaging. *Phys Med Biol*. 1980;25:751.
6. Doyle FH, Pennock JM, Banks LM, et al. Nuclear magnetic resonance imaging of the liver: initial experience. *Am J Roentgenol*. 1982;138:193–200. https://doi.org/10.2214/ajr.138.2.193.
7. Young I, Clarke G, Baffles D, Pennock J, Doyle F, Bydder G. Enhancement of relaxation rate with paramagnetic contrast agents in NMR imaging. *J Comput Tomogr*. 1981;5:543–547.
8. Carr DH, Brown J, Bydder GM, et al. Gadolinium-DTPA as a contrast agent in MRI: initial clinical experience in 20 patients. *Am J Roentgenol*. 1984;143:215–224. https://doi.org/10.2214/ajr.143.2.215.
9. Stark DD, Felder RC, Wittenberg J, et al. Magnetic resonance imaging of cavernous hemangioma of the liver: tissue-specific characterization. *Am J Roentgenol*. 1985;145:213–222. https://doi.org/10.2214/ajr.145.2.213.
10. Edelman RR, Siegel JB, Singer A, Dupuis K, Longmaid HE. Dynamic MR imaging of the liver with gd-DTPA: initial clinical results. *Am J Roentgenol*. 1989;153:1213–1219. https://doi.org/10.2214/ajr.153.6.1213.
11. Semelka RC, Shoenut JP, Kroeker MA, et al. Focal liver disease: comparison of dynamic contrast-enhanced CT and T2-weighted fat-suppressed, FLASH, and dynamic gadolinium-enhanced MR imaging at 1.5 T. *Radiology*. 1992;184:687–694. https://doi.org/10.1148/radiology.184.3.1324509.
12. Earls JP, Krinsky GA. Abdominal and pelvic applications of opposed-phase MR imaging. *Am J Roentgenol*. 1997;169:1071–1077. https://doi.org/10.2214/ajr.169.4.9308467.
13. Merkle EM, Nelson RC. Dual gradient-echo in-phase and opposed-phase hepatic MR imaging: a useful tool for evaluating more than fatty infiltration or fatty sparing. *Radiographics*. 2006;26:1409–1418.
14. Jeong YY, Mitchell DG, Holland GA. Liver lesion conspicuity: T2-weighted breath-hold fast spin-echo MR imaging before and after gadolinium enhancement—initial experience. *Radiology*. 2001;219:455–460.
15. Ito K, Mitchell DG, Outwater EK, Szklaruk J, Sadek AG. Hepatic lesions: discrimination of nonsolid, benign lesions from solid, malignant lesions with heavily T2-weighted fast spin-echo MR imaging. *Radiology.*. 1997;204:729–737.
16. Griffin N, Charles-Edwards G, Grant LA. Magnetic resonance cholangiopancreatography: the ABC of MRCP. *Insights Imaging*. 2012;3:11–21.
17. Malayeri AA, El Khouli RH, Zaheer A, et al. Principles and applications of diffusion-weighted imaging in cancer detection, staging, and treatment follow-up. *Radiographics*. 2011;31:1773–1791.

18. Guglielmo FF, Kania LM, Ahmad HM, Roth CG, Mitchell DG. Interpreting body MRI cases: what you need to know to get started. *Abdom Radiol*. 2016;41:2248–2269.
19. Taouli B, Koh D. Diffusion-weighted MR imaging of the Liver1. *Radiology*. 2010;254:47–66.
20. Guglielmo FF, Mitchell DG, Gupta S. Gadolinium contrast agent selection and optimal use for body MR imaging. *Radiol Clin North Am*. 2014;52:637–656.
21. Tweedle MF, Kanal E, Muller R. Considerations in the selection of a new gadolinium-based contrast agent. *Appl Radiol*. 2014;43:1–11.
22. van der Molen AJ, Bellin MF. Extracellular gadolinium-based contrast media: differences in diagnostic efficacy. *Eur J Radiol*. 2008;66:168–174.
23. Frydrychowicz A, Lubner MG, Brown JJ, et al. Hepatobiliary MR imaging with gadolinium-based contrast agents. *J Magn Reson Imaging*. 2012;35:492–511.
24. Goodwin MD, Dobson JE, Sirlin CB, Lim BG, Stella DL. Diagnostic challenges and pitfalls in MR imaging with hepatocyte-specific contrast agents. *Radiographics*. 2011;31:1547–1568.
25. Lewis M, Yanny S, Malcolm PN. Advantages of blood pool contrast agents in MR angiography: a pictorial review. *J Med Imaging Radiat Oncol*. 2012;56:187–191. https://doi.org/10.1111/j.1754-9485.2012.02347.x.
26. Hadizadeh DR, Gieseke J, Lohmaier SH, et al. Peripheral MR angiography with blood pool contrast agent: prospective intraindividual comparative study of high-spatial-resolution steady-state MR angiography versus standard-resolution first-pass MR angiography and DSA. *Radiology*. 2008;249:701–711.
27. Umschaden HW, Szolar D, Gasser J, Umschaden M, Haselbach H. Small-bowel disease: comparison of MR enteroclysis images with conventional enteroclysis and surgical findings. *Radiology*. 2000;215:717–725.
28. Low RN. Abdominal MRI advances in the detection of liver tumours and characterisation. *Lancet Oncol*. 2007;8:525–535.
29. Brenner DJ, Hall EJ. Computed tomography—an increasing source of radiation exposure. *N Engl J Med*. 2007;357:2277–2284.
30. Ramalho M, Herédia V, Cardoso C, et al. Magnetic resonance imaging of small bowel Crohn's disease. *Acta Med Port*. 2012;25:231–240.
31. Cronin CG, Lohan DG, Browne AM, Roche C, Murphy JM. Does MRI with oral contrast medium allow single-study depiction of inflammatory bowel disease enteritis and colitis? *Eur Radiol*. 2010;20:1667–1674.
32. Schwartz DA, Wiersema MJ, Dudiak KM, et al. A comparison of endoscopic ultrasound, magnetic resonance imaging, and exam under anesthesia for evaluation of Crohn's perianal fistulas. *Gastroenterology*. 2001;121:1064–1072.
33. Froehlich JM, Patak MA, von Weymarn C, Juli CF, Zollikofer CL, Wentz K. Small bowel motility assessment with magnetic resonance imaging. *J Magn Reson Imaging*. 2005;21:370–375.
34. Liu B, Ramalho M, AlObaidy M, et al. Gastrointestinal imaging-practical magnetic resonance imaging approach. *World J Radiol*. 2014;6:544–566. https://doi.org/10.4329/wjr.v6.i8.544.
35. Itai Y, Ohtomo K, Furui S, Yamauchi T, Minami M, Yashiro N. Noninvasive diagnosis of small cavernous hemangioma of the liver: advantage of MRI. *Am J Roentgenol*. 1985;145:1195–1199. https://doi.org/10.2214/ajr.145.6.1195.
36. Wittenberg J, Stark DD, Forman BH, et al. Differentiation of hepatic metastases from hepatic hemangiomas and cysts by using MR imaging. *Am J Roentgenol*. 1988;151:79–84. https://doi.org/10.2214/ajr.151.1.79.
37. Lombardo DM, Baker ME, Spritzer CE, Blinder R, Meyers W, Herfkens RJ. Hepatic hemangiomas vs metastases: MR differentiation at 1.5 T. *Am J Roentgenol*. 1990;155:55–59. https://doi.org/10.2214/ajr.155.1.2112864.
38. Mitchell DG, Saini S, Weinreb J, et al. Hepatic metastases and cavernous hemangiomas: Distinction with standard- and triple-dose gadoteridol-enhanced MR imaging. *Radiology*. 1994;193:49–57. https://doi.org/10.1148/radiology.193.1.8090921.
39. Seo HJ, Kim MJ, Lee JD, Chung WS, Kim YE. Gadoxetate disodium-enhanced magnetic resonance imaging versus contrast-enhanced 18F-fluorodeoxyglucose positron emission tomography/computed tomography for the detection of colorectal liver metastases. *Invest Radiol*. 2011;46:548–555. https://doi.org/10.1097/RLI.0b013e31821a2163.
40. Muhi A, Ichikawa T, Motosugi U, et al. Diagnosis of colorectal hepatic metastases: Comparison of contrast-enhanced CT, contrast-enhanced US, superparamagnetic iron oxide-enhanced MRI, and gadoxetic acid-enhanced MRI. *J Magn Reson Imaging*. 2011;34:326–335.
41. Haradome H, Grazioli L, Tsunoo M, Motosugi U, Kwee TC, Takaraha T. Gadoxetic acid disodium-enhanced hepatocyte phase MRI: can increasing the flip angle improve focal liver lesion detection? *J Magn Reson Imaging*. 2012;35:132–139.
42. Bieze M, van den Esschert JW, Nio CY, et al. Diagnostic accuracy of MRI in differentiating hepatocellular adenoma from focal nodular hyperplasia: prospective study of the additional value of gadoxetate disodium. *Am J Roentgenol*. 2012;199:26–34.
43. Grieser C, Steffen IG, Seehofer D, et al. Histopathologically confirmed focal nodular hyperplasia of the liver: gadoxetic acid-enhanced MRI characteristics. *Magn Reson Imaging*. 2013;31:755–760.
44. Gupta RT, Iseman CM, Leyendecker JR, Shyknevsky I, Merkle EM, Taouli B. Diagnosis of focal nodular hyperplasia with MRI: multicenter retrospective study comparing gadobenate dimeglumine to gadoxetate disodium. *Am J Roentgenol*. 2012;199:35–43.
45. Roberts LR, Sirlin CB, Zaiem F, et al. Imaging for the diagnosis of hepatocellular carcinoma: a systematic review and meta-analysis. *Hepatology*. 2018;67:401–421.
46. Saranathan M, Rettmann DW, Hargreaves BA, et al. Differential subsampling with Cartesian ordering (DISCO): a high spatio-temporal resolution Dixon imaging sequence for multiphasic contrast enhanced abdominal imaging. *J Magn Reson Imaging*. 2012;35:1484–1492.
47. El-Serag HB. Hepatocellular carcinoma: Recent trends in the united states. *Gastroenterology*. 2004;127:S27–S34.
48. El-Serag HB. Current concepts. *N Engl J Med*. 2011;365:1118–1127.
49. Fattovich G, Stroffolini T, Zagni I, Donato F. Hepatocellular carcinoma in cirrhosis: incidence and risk factors. *Gastroenterology*. 2004;127:S35–S50.
50. Llovet JM, Fuster J, Bruix J. Intention-to-treat analysis of surgical treatment for early hepatocellular carcinoma: resection versus transplantation. *Hepatology*. 1999;30:1434–1440.
51. Fong Y, Sun RL, Jarnagin W, Blumgart LH. An analysis of 412 cases of hepatocellular carcinoma at a western center. *Ann Surg*. 1999;229:790–799. **(discussion 799–800)**.
52. Bruix J, Sherman M. Management of hepatocellular carcinoma: an update. *Hepatology*. 2011;53:1020–1022.
53. Mazzaferro V, Regalia E, Doci R, et al. Liver transplantation for the treatment of small hepatocellular carcinomas in patients with cirrhosis. *N Engl J Med*. 1996;334:693–700.
54. Chan SC. Liver transplantation for hepatocellular carcinoma. *Liver Cancer*. 2013;2:338–344. https://doi.org/10.1159/000343849.
55. Ramalho M, Matos AP, AlObaidy M, Velloni F, Altun E, Semelka RC. Magnetic resonance imaging of the cirrhotic liver:

diagnosis of hepatocellular carcinoma and evaluation of response to treatment—part 2. *Radiol Bras*. 2017;50:115–125.
56. Jha RC, Mitchell DG, Weinreb JC, et al. LI-RADS categorization of benign and likely benign findings in patients at risk of hepatocellular carcinoma: a pictorial atlas. *Am J Roentgenol*. 2014;203:W48–W69.
57. Tang A, Cruite I, Mitchell DG, et al. Hepatocellular carcinoma imaging systems: why they exist, how they evolved, and how they differ. *Abdom Radiol*. 2018;43:3–12.
58. Bret PM, Labadie M, Bretagnolle M, et al. Hepatocellular carcinoma: diagnosis by percutaneous fine needle biopsy. *Gastrointest Radiol*. 1988;13:253–255.
59. Giorgio A, Tarantino L, de Stefano G, et al. Complications after interventional sonography of focal liver lesions: a 22-year single-center experience. *J Ultrasound Med*. 2003;22:193–205.
60. Caturelli E, Solmi L, Anti M, et al. Ultrasound guided fine needle biopsy of early hepatocellular carcinoma complicating liver cirrhosis: a multicentre study. *Gut*. 2004;53:1356–1362.
61. Scholmerich J, Schacherer D. Diagnostic biopsy for hepatocellular carcinoma in cirrhosis: useful, necessary, dangerous, or academic sport? *Gut*. 2004;53:1224–1226.
62. Forner A, Vilana R, Ayuso C, et al. Diagnosis of hepatic nodules 20 mm or smaller in cirrhosis: prospective validation of the noninvasive diagnostic criteria for hepatocellular carcinoma. *Hepatology*. 2008;47:97–104.
63. Durand F, Regimbeau JM, Belghiti J, et al. Assessment of the benefits and risks of percutaneous biopsy before surgical resection of hepatocellular carcinoma. *J Hepatol*. 2001;35:254–258.
64. Takamori R, Wong LL, Dang C, et al. Needle-tract implantation from hepatocellular cancer: is needle biopsy of the liver always necessary? *Liver Transpl*. 2000;6:67–72.
65. Silva MA, Hegab B, Hyde C, et al. Needle track seeding following biopsy of liver lesions in the diagnosis of hepatocellular cancer: a systematic review and meta-analysis. *Gut*. 2008;57:1592–1596.
66. Stigliano R, Marelli L, Yu D, et al. Seeding following percutaneous diagnostic and therapeutic approaches for hepatocellular carcinoma. What is the risk and the outcome? Seeding risk for percutaneous approach of HCC. *Cancer Treat Rev*. 2007;33:437–447.
67. Ronot M, Fouque O, Esvan M, et al. Comparison of accuracy of AASLD and LI-RADS criteria for the non-invasive diagnosis of HCC smaller than 3 cm. *J Hepatol*. 2017; Available online 21 December 2017, Accessed February 18, 2018. https://doi.org/10.1016/j.jhep.2017.12.014.
68. Liu W, Qin J, Guo R, et al. Accuracy of the diagnostic evaluation of hepatocellular carcinoma with LI-RADS. *Acta Radiol*. 2018;59:140–146.
69. Mitchell DG, Bashir MR, Sirlin CG. Management implications and outcomes of LI-RADS-2, -3, -4 and -M lesions. *Abdom Radiol*. 2018;43:143–148.
70. Mitchell DG, Bruix J, Sherman M, Sirlin CB. LI-RADS (liver imaging reporting and data system): Summary, discussion, and consensus of the LI-RADS management working group and future directions. *Hepatology*. 2015;61:1056–1065.
71. Llovet JM, Bruix J. Systematic review of randomized trials for unresectable hepatocellular carcinoma: chemoembolization improves survival. *Hepatology*. 2003;37:429–442.
72. Roth CG, Mitchell DG. Hepatocellular carcinoma and other hepatic malignancies: MR imaging. *Radiol Clin North Am*. 2014;52:683–707.
73. Younossi ZM, Stepanova M, Afendy M, et al. Changes in the prevalence of the most common causes of chronic liver diseases in the united states from 1988 to 2008. *Clin Gastroenterol Hepatol*. 2011;9:e1.
74. Chen J, Yin M, Glaser KJ, Talwalkar JA, Ehman RL. MR elastography of liver disease: state of the art. *Appl Radiol*. 2013;42:5–12.
75. Venkatesh SK, Ehman RL. Magnetic resonance elastography of liver. *Magn Reson Imaging Clin N Am*. 2014;22:433–446.
76. Bedossa P, Dargère D, Paradis V. Sampling variability of liver fibrosis in chronic hepatitis C. *Hepatology*. 2003;38:1449–1457.
77. Regev A, Berho M, Jeffers LJ, et al. Sampling error and intraobserver variation in liver biopsy in patients with chronic HCV infection. *Am J Gastroenterol*. 2002;97:2614–2618.
78. West J, Card TR. Reduced mortality rates following elective percutaneous liver biopsies. *Gastroenterology*. 2010;139:1230–1237.
79. Venkatesh SK, Yin M, Takahashi N, Glockner JF, Talwalkar JA, Ehman RL. Non-invasive detection of liver fibrosis: MR imaging features vs MR elastography. *Abdom Imaging*. 2015;40:766–775.
80. Yin M, Talwalkar JA, Glaser KJ, et al. Assessment of hepatic fibrosis with magnetic resonance elastography. *Clin Gastroenterol Hepatol*. 2007;5:e2.
81. Chalasani N, Younossi Z, Lavine JE, et al. The diagnosis and management of nonalcoholic fatty liver disease: Practice guideline by the American association for the study of liver diseases, American college of gastroenterology, and the American gastroenterological association. *Hepatology*. 2012;55:2005–2023.
82. Charlton MR, Burns JM, Pedersen RA, Watt KD, Heimbach JK, Dierkhising RA. Frequency and outcomes of liver transplantation for nonalcoholic steatohepatitis in the united states. *Gastroenterology*. 2011;141:1249–1253.
83. Starley BQ, Calcagno CJ, Harrison SA. Nonalcoholic fatty liver disease and hepatocellular carcinoma: a weighty connection. *Hepatology*. 2010;51:1820–1832.
84. Kinner S, Reeder SB, Yokoo T. Quantitative imaging biomarkers of NAFLD. *Dig Dis Sci*. 2016;61:1337–1347.
85. Reeder SB, Sirlin CB. Quantification of liver fat with magnetic resonance imaging. *Magn Reson Imaging Clin N Am*. 2010;18:337–357.
86. Reeder SB, Cruite I, Hamilton G, Sirlin CB. Quantitative assessment of liver fat with magnetic resonance imaging and spectroscopy. *J Magn Reson Imaging*. 2011;34:729–749.
87. Idilman IS, Aniktar H, Idilman R, et al. Hepatic steatosis: quantification by proton density fat fraction with MR imaging versus liver biopsy. *Radiology*. 2013;267:767–775.
88. Sirlin CB, Reeder SB. Magnetic resonance imaging quantification of liver iron. *Magn Reson Imaging Clin N Am*. 2010;18:359–381.
89. Anderson ER, Shah YM. Iron homeostasis in the liver. *Compr Physiol*. 2013;3:315–330.
90. Wallner BK, Schumacher KA, Weidenmaier W, Friedrich JM. Dilated biliary tract: evaluation with MR cholangiography with a T2-weighted contrast-enhanced fast sequence. *Radiology*. 1991;181:805–808. https://doi.org/10.1148/radiology.181.3.1947101.
91. Varghese J, Farrell M, Courtney G, Osborne H, Murray F, Lee M. A prospective comparison of magnetic resonance cholangiopancreatography with endoscopic retrograde cholangiopancreatography in the evaluation of patients with suspected biliary tract disease. *Clin Radiol*. 1999;54:513–520.
92. Guibaud L, Bret PM, Reinhold C, Atri M, Barkun AN. Diagnosis of choledocholithiasis: Value of MR cholangiography. *Am J Roentgenol*. 1994;163:847–850. https://doi.org/10.2214/ajr.163.4.8092021.
93. Boraschi P, Neri E, Braccini G, et al. Choledocolithiasis: diagnostic accuracy of MR cholangiopancreatography. Three-year experience. *Magn Reson Imaging*. 1999;17:1245–1253.
94. Coakley FV, Schwartz LH. Magnetic resonance cholangiopancreatography. *J Magn Reson Imaging*. 1999;9:157–162.

95. Margulis AR, Fisher MR. Present clinical status of magnetic resonance imaging. *Magn Reson Med*. 1985;2:309–327.
96. Chezmar JL, Nelson RC, Small WC, Bernardino ME. Magnetic resonance imaging of the pancreas with gadolinium-DTPA. *Abdom Imaging*. 1991;16:139–142.
97. Semelka RC, Ascher SM. MR imaging of the pancreas. *Radiology*. 1993;188:593–602. https://doi.org/10.1148/radiology.188.3.8351317.
98. Miller FH, Rini NJ, Keppke AL. MRI of adenocarcinoma of the pancreas. *Am J Roentgenol*. 2006;187:W365–W374.
99. Ichikawa T, Sou H, Araki T, et al. Duct-penetrating sign at MRCP: Usefulness for differentiating inflammatory pancreatic mass from pancreatic carcinomas. *Radiology*. 2001;221:107–116.
100. Lemke A, Laun FB, Klauss M, et al. Differentiation of pancreas carcinoma from healthy pancreatic tissue using multiple b-values: comparison of apparent diffusion coefficient and intravoxel incoherent motion derived parameters. *Invest Radiol*. 2009;44:769–775. https://doi.org/10.1097/RLI.0b013e3181b62271.
101. Cho SG, Lee DH, Lee KY, et al. Differentiation of chronic focal pancreatitis from pancreatic carcinoma by in vivo proton magnetic resonance spectroscopy. *J Comput Assist Tomogr*. 2005;29:163–169.
102. Fidler J. MR imaging of the small bowel. *Radiol Clin North Am*. 2007;45:317–331.
103. Fidler JL, Guimaraes L, Einstein DM. MR imaging of the small bowel. *Radiographics*. 2009;29:1811–1825.
104. Young BM, Fletcher JG, Booya F, et al. Head-to-head comparison of oral contrast agents for cross-sectional enterography: Small bowel distention, timing, and side effects. *J Comput Assist Tomogr*. 2008;32:32–38. https://doi.org/10.1097/RCT.0b013e318061961d.
105. Masselli G, Gualdi G. MR imaging of the small bowel. *Radiology*. 2012;264:333–348.
106. Gandhi SN, Brown MA, Wong JG, Aguirre DA, Sirlin CB. MR contrast agents for liver imaging: what, when, how. *Radiographics*. 2006;26:1621–1636.
107. Wnorowski AM, Guglielmo FF, Mitchell DG. How to perform and interpret cine MR enterography. *J Magn Reson Imaging*. 2015;42:1180–1189.
108. Grand DJ, Guglielmo FF, Al-Hawary MM. MR enterography in Crohn's disease: Current consensus on optimal imaging technique and future advances from the SAR crohn's disease-focused panel. *Abdom Imaging*. 2015;40:953–964.
109. Lee SS, Kim AY, Yang S, et al. Crohn disease of the small bowel: comparison of CT enterography, MR enterography, and small-bowel follow-through as diagnostic techniques. *Radiology*. 2009;251:751–761.
110. Samuel S, Bruining DH, Loftus EV, et al. Endoscopic skipping of the distal terminal ileum in crohn's disease can lead to negative results from ileocolonoscopy. *Clin Gastroenterol Hepatol*. 2012;10:1253–1259.
111. Fletcher JG, Fidler JL, Bruining DH, Huprich JE. New concepts in intestinal imaging for inflammatory bowel diseases. *Gastroenterology*. 2011;140:e7.
112. Siddiki HA, Fidler JL, Fletcher JG, et al. Prospective comparison of state-of-the-art MR enterography and CT enterography in small-bowel crohn's disease. *Am J Roentgenol*. 2009;193:113–121.
113. Bruining DH, Siddiki HA, Fletcher JG, Tremaine WJ, Sandborn WJ, Loftus EV. Prevalence of penetrating disease and extraintestinal manifestations of crohn's disease detected with CT enterography. *Inflamm Bowel Dis*. 2008;14:1701–1706.
114. Taylor FG, Swift RI, Blomqvist L, Brown G. A systematic approach to the interpretation of preoperative staging MRI for rectal cancer. *Am J Roentgenol*. 2008;191:1827–1835.
115. Patel UB, Taylor F, Blomqvist L, et al. Magnetic resonance imaging–detected tumor response for locally advanced rectal cancer predicts survival outcomes: MERCURY experience. *J Clin Oncol*. 2011;29:3753–3760.
116. de Miguel Criado J, del Salto LG, Rivas PF, et al. MR imaging evaluation of perianal fistulas: spectrum of imaging features. *Radiographics*. 2011;32:175–194.
117. Morris J, Spencer JA, Ambrose NS. MR imaging classification of perianal fistulas and its implications for patient management. *Radiographics*. 2000;20:623–635.
118. Gecse KB, Bemelman W, Kamm MA, et al. A global consensus on the classification, diagnosis and multidisciplinary treatment of perianal fistulising crohn's disease. *Gut*. 2014;63:1381–1392. https://doi.org/10.1136/gutjnl-2013-306709.
119. Pedrosa I, Lafornara M, Pandharipande PV, Goldsmith JD, Rofsky NM. Pregnant patients suspected of having acute appendicitis: effect of MR imaging on negative laparotomy rate and appendiceal perforation rate. *Radiology*. 2009;250:749–757.
120. Pedrosa I, Levine D, Eyvazzadeh AD, Siewert B, Ngo L, Rofsky NM. MR imaging evaluation of acute appendicitis in pregnancy. *Radiology*. 2006;238:891–899.
121. Abrigo JM, Shen J, Wong VW, et al. Nonalcoholic fatty liver disease: spectral patterns observed from an in vivo phosphorus magnetic resonance spectroscopy study. *J Hepatol*. 2014;60:809–815.
122. Traussnigg S, Kienbacher C, Gajdošík M, et al. P1045: ultra-high-field MR-spectroscopy in NAFLD as non-invasive in-vivo tool for monitoring changes in fat and energy metabolism with potential identification of NASH and advanced fibrosis by saturation transfer technique. *J Hepatol*. 2015;62:S739–S740.
123. Dezortova M, Taimr P, Skoch A, Spicak J, Hajek M. Etiology and functional status of liver cirrhosis by 31P MR spectroscopy. *World J Gastroenterol*. 2005;11:6926–6931.
124. Purvis LA, Clarke WT, Valkovič L, et al. Phosphodiester content measured in human liver by in vivo 31P MR spectroscopy at 7 tesla. *Magn Reson Med*. 2017;78:2095–2105.